The Deep Plumbing System of Ischia: a Physico-chemical Window on the Fluid-saturated and CO$_2$-sustained Neapolitan Volcanism (Southern Italy)

ROBERTO MORETTI[1,2,]*, ILENIA ARIENZO[2], GIOVANNI ORSI[2], LUCIA CIVETTA[2,3] AND MASSIMO D'ANTONIO[2,3]

[1]DIPARTIMENTO DI INGEGNERIA CIVILE, DESIGN, EDILIZIA E AMBIENTE, SECONDA UNIVERSITÀ DEGLI STUDI DI NAPOLI, VIA ROMA 29, 81031 AVERSA (CE), ITALY

[2]ISTITUTO NAZIONALE DI GEOFISICA E VULCANOLOGIA, SEZIONE DI NAPOLI OSSERVATORIO VESUVIANO, VIA DIOCLEZIANO 328, 80124 NAPOLI, ITALY

[3]DIPARTIMENTO DI SCIENZE DELLA TERRA, DELL'AMBIENTE E DELLE RISORSE, UNIVERSITÀ DEGLI STUDI DI NAPOLI 'FEDERICO II', LARGO SAN MARCELLINO, 80138 NAPOLI, ITALY

Ischia, a volcanic island located 18 miles SW of Naples (Southern Italy), is a densely populated active caldera that last erupted in AD 1302. Melt inclusions in phenocrysts of the Vateliero and Cava Nocelle shoshonite–latite eruptive products (6th to 4th centuries BC) constrain the structure and nature of the Ischia deep magmatic feeding system. Their geochemical characteristics make Ischia a natural borehole for probing the physico-chemical conditions of magma generation in mantle contaminated by slab-derived fluids or melts, largely dominated by CO$_2$. Volatile concentrations in olivine-hosted melt inclusions require gas–melt equilibria at between 3 and 18 km depth. In agreement with what has already been demonstrated at the other neighboring Neapolitan volcanoes (Procida, Campi Flegrei caldera and Somma–Vesuvius volcanic complex), a major crystallization depth at 8–10 km has been identified. The analyzed melt inclusions provide clear evidence for CO$_2$-dominated gas fluxing and consequent dehydration of magma batches stagnating at crustal discontinuities. Gas fluxing is further supported by selective enrichment in K owing to fluid-transfer during magma differentiation. This takes place under oxidized conditions ($Fe^{3+}/\Sigma Fe \geq 0\cdot3$) that can be fixed by an equimolar proportion of divalent and trivalent iron in the melt if post-entrapment crystallization of the host olivine is discarded. The melt inclusion data, together with data from the literature for other Neapolitan volcanoes, show that magmatism and volcanism in the Neapolitan area, despite differences in composition and eruption dynamics, are closely linked to supercritical CO$_2$-rich fluids. These fluids are produced by devolatilization of subducting terrigenous–pelagic metasediments and infiltrate the overlying mantle wedge, generate magmas and control their ascent up to eruption. Geochemical characteristics of Ischia and the other Neapolitan volcanoes reveal that the extent of fluid or melt contamination of the pre-subduction asthenospheric mantle wedge was similar among these volcanoes. However, differences in the isotopic compositions of the erupted magmas (more enriched in radiogenic Sr at Ischia, Campi Flegrei and Somma–Vesuvius with respect to Procida) and the amount of H$_2$O in the plumbing system of these volcanoes (almost double at Ischia, Campi Flegrei and Somma–Vesuvius than at Procida) reflect the different flow-rates of deep slab-derived fluids or melts through the mantle wedge, which, in turn, control the amount of generated magma. The high bulk permeability of the lithosphere below Ischia, Campi Flegrei and Somma–Vesuvius, determined by the occurrence of intersecting NW–SE and NE–SW regional fault systems, favours fluid ascent and accumulation at crustal levels, with consequent larger magma production and storage than at Procida, located along the NE–SW system.

KEY WORDS: *CO$_2$-fluxing; melt inclusions; redox state; trachybasalts; alkali enrichment*

*Corresponding author. Present address: Dipartimento di Ingegneria Civile, Design, Edilizia e Ambiente, Seconda Università degli Studi di Napoli, Via Roma 29, 81031 Aversa (CE), Italy. Telephone and fax: 00390815010416. E-mail: roberto.moretti@unina2.it

INTRODUCTION

Melt inclusions (MI) are droplets of melt trapped in phenocrysts (e.g. Roedder, 1984) along the pathways of magma evolution from deep to shallow zones of segregation and storage, up to extrusion. As such, they provide fundamental clues to and quantitative constraints on the physico-chemical conditions of magma storage, ascent and pre-eruptive degassing (e.g. Anderson *et al.*, 1989; Métrich & Clocchiatti, 1989; Blundy & Cashman, 2008; Barsanti *et al.*, 2009). The chemical compositions of MI are a powerful geochemical tool with which to characterize the magmatic feeding system of a volcano, providing data that can be integrated with the results of geophysical investigations. MI studies have become essential in understanding and quantifying magmatic processes, contributing to assessments of volcanic hazard at active volcanoes and particularly for defining likely eruption scenarios involving magma recharge over short to medium timescales (e.g. years to tens of years). MI-based retrieval of the gas composition coexisting with the melt at depth can represent a highly valuable complement to gas discharge measurements at surface (e.g. Aiuppa *et al.*, 2010; Arienzo *et al.*, 2010) and provide an essential tool to solve ambiguities concerning the magmatic versus hydrothermal origin of gas emissions at volcanic sites (e.g. Chiodini *et al.*, 2006).

The island of Ischia is a densely populated resurgent caldera in the Gulf of Naples (Southern Italy) (Fig. 1). The last eruption was in AD 1302 and there has been ground deformation in historical times, recent seismicity and diffuse fumarolic and thermal-spring activity; these provide evidence for the state of activity of the magmatic feeding system, as well as information on hydrothermal potential and volcanic hazard (Buchner *et al.*, 1996; Orsi *et al.*, 2003; Sepe *et al.*, 2007; Sbrana *et al.*, 2009; Di Napoli *et al.*, 2011).

In such a framework, assessment of the processes occurring at variable depths within the magmatic feeding system is clearly an important task for the scientific community. In this study we have focused on MI in the products of eruptions fed by weakly differentiated magmas over the last 3 kyr. The specific aims were the definition of the architecture of the magmatic feeding system and evaluation of the relationships between deep and shallow transfer processes of subduction-related fluids or melts. The latter have been addressed by modelling the oxidation state and degassing processes within a CO_2–H_2O–H_2S–SO_2–silicate melt system and by discussing the variability of alkalis and halogens, to define the role played by fluids in driving magma ascent to the surface. In addition, we have explored the geochemical similarities and differences between Ischia and the other Neapolitan volcanoes and interpreted them in the context of the structural setting of the area, providing insights into the geodynamic processes that control the Neapolitan magmatism.

GEOLOGICAL, PETROLOGICAL AND GEOCHEMICAL BACKGROUND OF ISCHIA

Ischia is the emergent top of a large volcanic complex that rises more than 1000 m above the sea floor. Together with Campi Flegrei (CF), Procida and Somma–Vesuvius (SV), it is one of the four Neapolitan volcanoes formed in the graben of the Campanian Plain along the Tyrrhenian Sea margin of the Apennines (Fig. 1) (Orsi *et al.*, 2003; Peccerillo, 2005). This margin has been affected by extensional processes since the Miocene as a consequence of the eastward migration of the Apennines in relation to a progressive eastward retreat of the subducting Ionian lithosphere (e.g. Jolivet *et al.*, 2009). Extension has occurred along mainly NW–SE normal and subordinate NE–SW transverse faults (Acocella & Funiciello, 2006, and references therein). Ischia, Procida and CF are NE–SW aligned and constitute the Phlegraean Volcanic District (PVD) (Orsi *et al.*, 1996a). The Ischia system, as well as those of CF and SV, is associated with a complex setting of tectonic and volcano-tectonic features, located at the intersection of the NE–SW- and NW–SE-trending regional fault systems (Acocella & Funiciello, 1999, 2006). The complex structural setting allows ascent of magmas as well as deep-to-shallow emplacement of major magma bodies. Ischia and CF are resurgent calderas (Orsi *et al.*, 1991, 1996a, 1999a; Acocella & Funiciello, 1999; Acocella *et al.*, 2004), SV is a strato-volcano (Santacroce *et al.*, 2008), and Procida is a monogenetic volcanic field (De Astis *et al.*, 2004).

At Ischia, volcanism began prior to 150 ka BP and has continued intermittently, with quiescent periods lasting centuries to millennia, until the last eruption in AD 1302 (Vezzoli, 1988; Orsi *et al.*, 1996b; de Vita *et al.*, 2010). The volcanic and deformation history is dominated by the caldera-forming Monte Epomeo Green Tuff (MEGT) eruption at *c.* 55 ka (Vezzoli, 1988), during a period of activity that generated the most voluminous and devastating eruptions of the island (Brown *et al.*, 2008, and references therein). The MEGT caldera floor was later affected by resurgence through a simple-shearing mechanism that generated uplift of about 900 m, probably over the past 33 kyr (the age of the oldest deformed rocks), and tilting of differentially displaced blocks; the most uplifted one is Monte Epomeo (Orsi *et al.*, 1991) (Fig. 1). The post-MEGT volcanic history has been subdivided into three periods of activity on the basis of structural and volcanological evidence, as well as geochemical and isotopic variations of the magmas erupted through time (Civetta *et al.*, 1991). During the last period of activity, which began 10 kyr ago, volcanism was mainly concentrated at around 5 ka and over the past 3 kyr. In this period resurgence dynamics have determined the conditions for magma ascent mainly
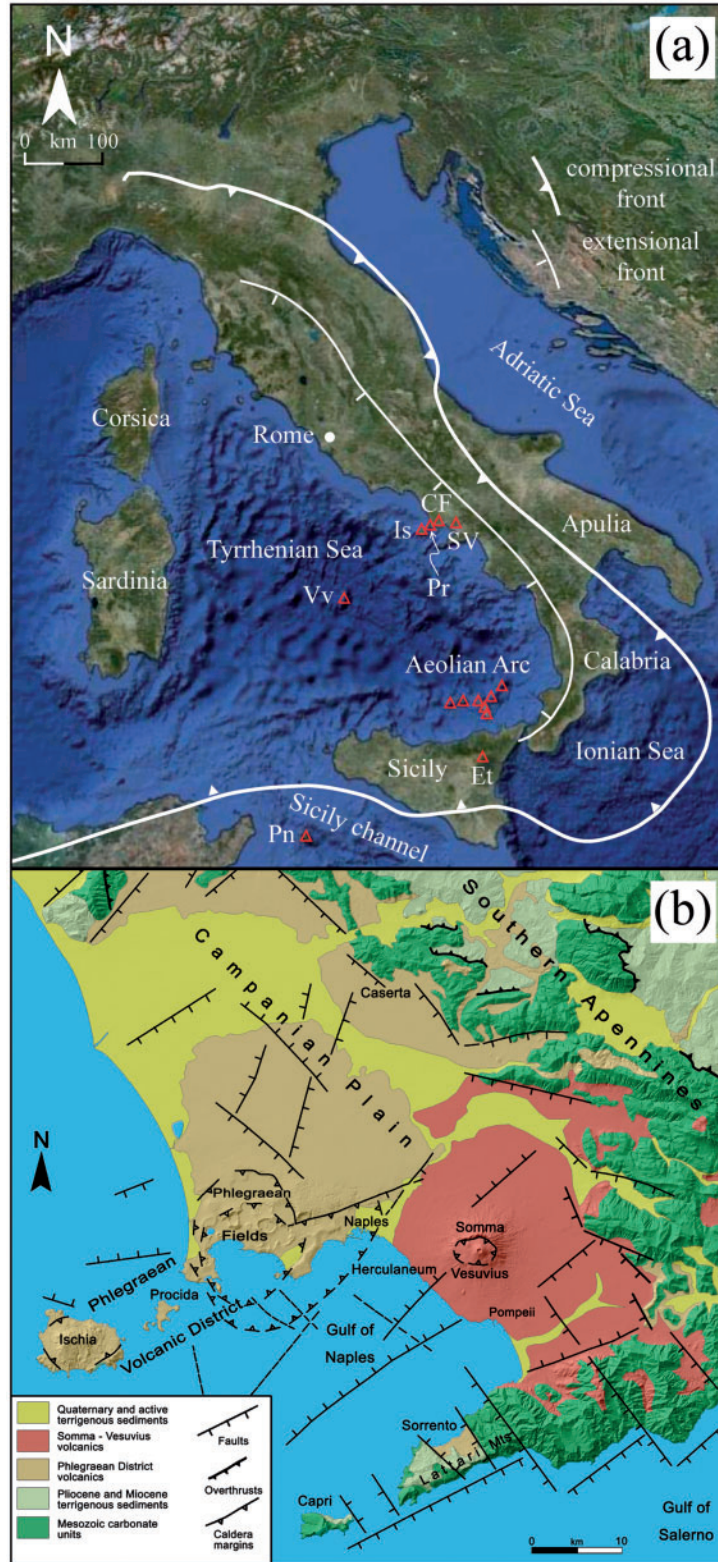
Fig. 1. (a) Traces of the subduction-related compression and extension fronts along the Apennine chain, modified after Acocella & Funiciello (2006). Is, Ischia; Pr, Procida; CF, Campi Flegrei; SV, Somma–Vesuvius; Vv, Vavilov; Et, Etna; Pn, Pantelleria. (b) Structural sketch map of the Campanian Plain and surrounding Apennines, modified after Orsi *et al.* (2003). (c) Geological sketch map of Ischia, modified after Orsi *et al.* (2003).
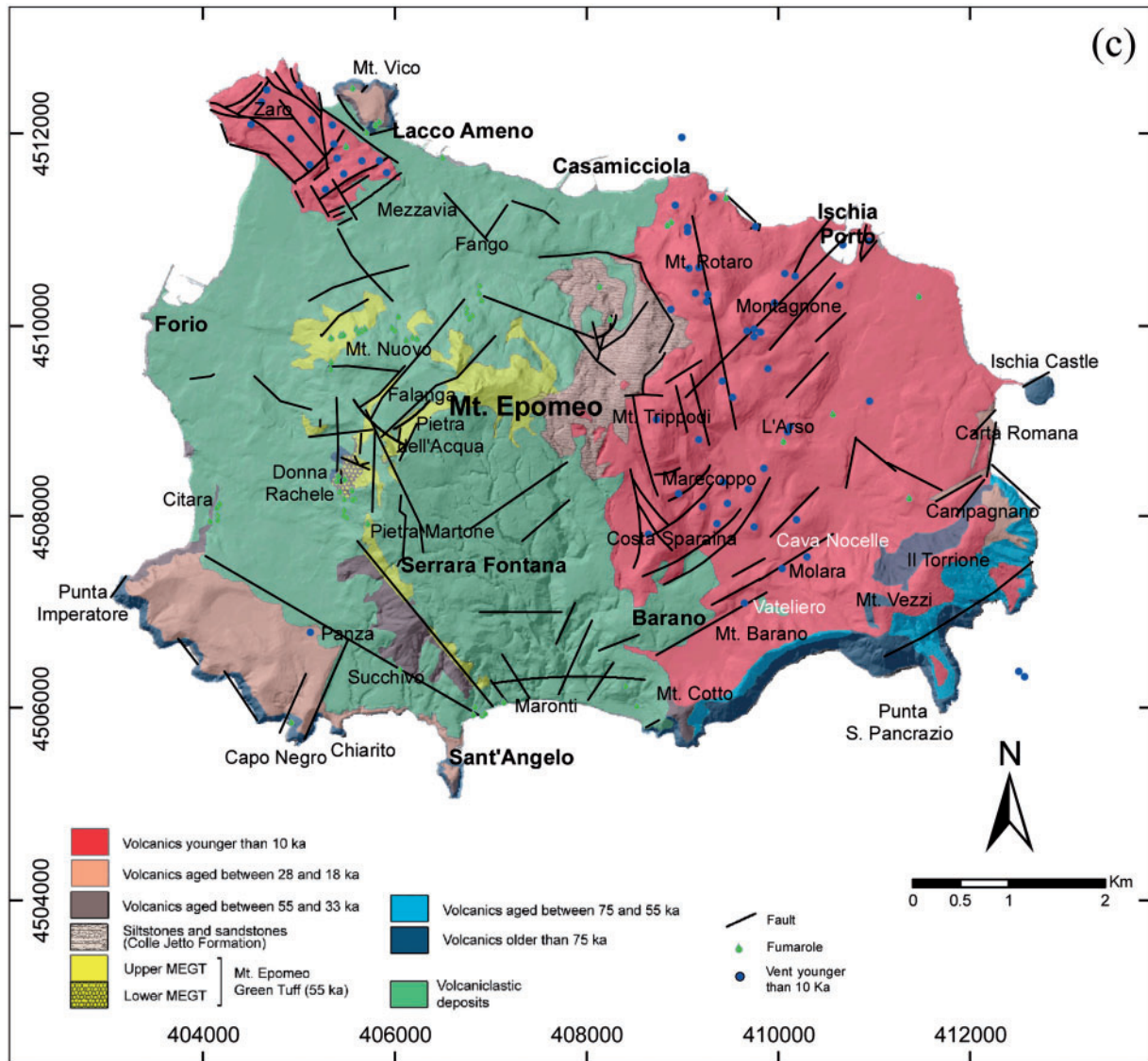
Fig. 1. (Continued).

to the east of the Monte Epomeo resurgent block, within the eastern sector of the island deformed by normal faults resulting from a tensile stress regime, and along portions of regional faults. The Molara, Vateliero and Cava Nocelle eruptions took place along the NE–SW-trending fault system delimiting the southeastern sector of the island towards the north (Fig. 1). This portion of the transfer system acted as marginal faults during the MEGT caldera collapse. These eruptions were low-magnitude explosive events, characterized by magmatic and phreatomagmatic explosions generating sequences of scoria fallout layers and ash-surge beds, intercalated with subordinate pumice fallout deposits (de Vita *et al.*, 2010). On the basis of stratigraphic, geochronological and archeological evidence, the Molara, Vateliero and Cava Nocelle eruptions followed each other at short time intervals between the 6th and 4th centuries BC (de Vita *et al.*, 2010, and references therein).

Ischia volcanic rocks vary in composition from shoshonite to phonolite (Fig. 2a); the most abundant rock type is trachyte. The least evolved magmas were erupted during the 28–18 ka period of activity (Grotta di Terra shoshonitic dike, 28 ka) and over the past 3 kyr (Molara, Vateliero, Cava Nocelle and Arso shoshonitic–latitic tephras; Fig. 1). The latter are characterized by petrographic, geochemical and isotopic features suggesting mingling or mixing among differently evolved, small magma batches, and entrapment of crystals inherited from previously erupted magmas (e.g. Civetta *et al.*, 1991; Piochi *et al.*, 1999; D'Antonio *et al.*, 2007, 2013).
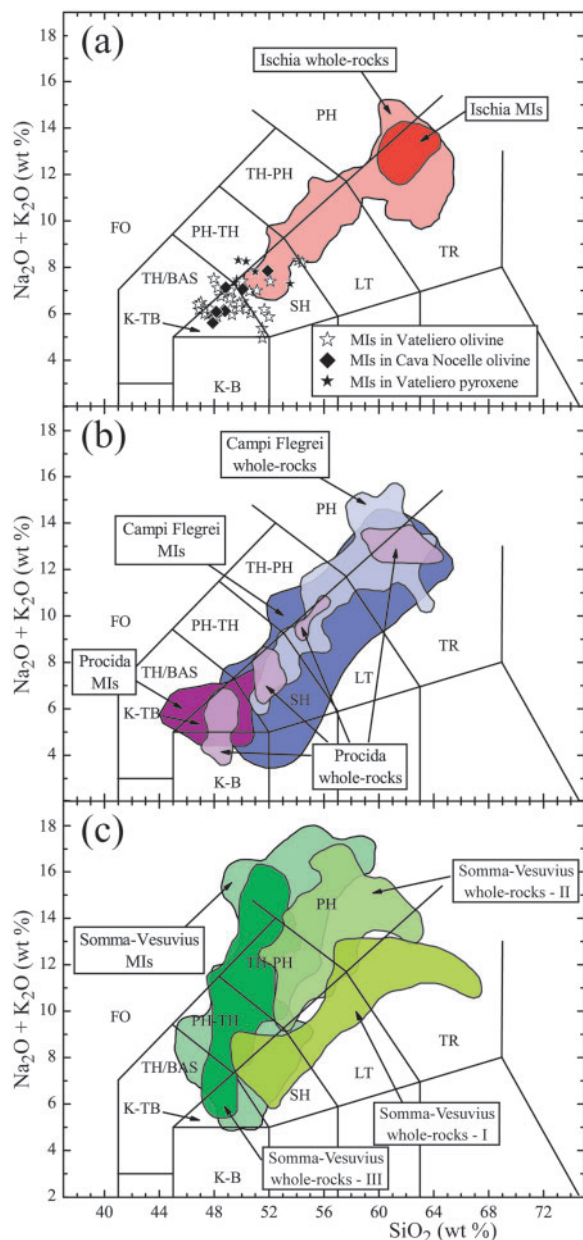
Fig. 2. (a) Total alkalis vs silica (TAS, Le Maitre *et al.*, 1989) diagram showing the compositions of the analyzed MI compared with the compositional fields of Ischia whole-rocks (Ghiara *et al.*, 1979; Vezzoli, 1988; Crisci *et al.*, 1989; Orsi *et al.*, 1992; Di Girolamo *et al.*, 1995; D'Antonio *et al.*, 2007; Brown *et al.*, 2008) and MI (Sbrana *et al.*, 2009) from the literature. (b) TAS diagram for CF and Procida whole-rocks and MI from the literature (D'Antonio *et al.*, 1999a, 1999b; Piochi *et al.*, 1999; Signorelli *et al.*, 1999a; Webster *et al.*, 2003; De Astis *et al.*, 2004; Fulignati *et al.*, 2004; Marianelli *et al.*, 2006; Cannatelli *et al.*, 2007; Severs, 2007; Mangiacapra *et al.*, 2008; Tonarini *et al.*, 2009; Arienzo *et al.*, 2010; Di Vito *et al.*, 2011; Mormone *et al.*, 2011). (c) TAS diagram for SV whole-rocks and MI from the literature (Cioni *et al.*, 1995, 1998; Belkin *et al.*, 1998; Marianelli *et al.*, 1999, 2005; Signorelli *et al.*, 1999b; Cioni, 2000; Di Renzo *et al.*, 2007; Fulignati & Marianelli, 2007; Santacroce *et al.*, 2008). SV whole-rocks I, II and III represent those emplaced between 22030 ± 175 and 19265 ± 105 yr cal BP, between 8890 ± 90 yr cal BP and AD 79, and between AD 79 and 1944, respectively (Santacroce *et al.*, 2008).

The deep structure of the Ischia caldera is poorly constrained. Modelling of magnetic data (Orsi *et al.*, 1999b) points to a large magma body at ∼7 km depth, which is either solidified or partly liquid, as the geothermal flux (Della Vedova *et al.*, 2001) suggests a solidus temperature of ∼1000°C at that depth. However, in the absence of seismic data, the role of petrology in assessing the characteristics of the deep magma storage system and magma crystallization depth is of fundamental importance. Eruption of shoshonitic to latitic magmas at the margin of the caldera and of differentiated magmas within it testifies to the ascent of weakly differentiated, CO_2-rich magmas of deep provenance along regional faults and the occurrence of a shallow magma storage region beneath the caldera, in which the magmas evolve to trachyte and phonolite. The trachyte and phonolite storage region is relatively shallow with respect to the reservoir from which the shoshonitic–latitic magmas come. This is suggested by phenocryst-hosted MI studies from the Ischia trachytes and phonolites (Sbrana *et al.*, 2009) that yielded H_2O contents up to 4 wt % but no CO_2 above the Fourier transform infrared (FTIR) spectroscopy detection limit. Accordingly, the occurrence of a relatively shallow magma reservoir (∼2 km deep) over the last few thousands of years below the caldera, filled by hot (1000°C) trachytic magma, has been suggested. Gravity and magnetic data point to the occurrence of an intrusive crystalline body, with few and sparse partially molten portions (Paoletti *et al.*, 2009), below the caldera. These data are consistent with petrological and isotopic data, which suggest that the volcanic activity of the last 5 kyr was fed by isotopically distinct small magma batches (Civetta *et al.*, 1991; Piochi *et al.*, 1999; D'Antonio *et al.*, 2007, 2013), which differentiated and mixed prior to extrusion.

The isotopic characteristics of dissolved gases in thermal waters demonstrate that the Ischia hydrothermal system is supplied by a deep-seated gas component, characterized by $CO_2 = 97 \cdot 7 \pm 1 \cdot 2$ vol. % (on a water-free basis), $\delta^{13}CO_2 = -3 \cdot 51 \pm 0 \cdot 9$‰, and $^3He/^4He \sim 3 \cdot 5$ Ra, probably of magmatic origin (Di Napoli *et al.*, 2009; 2011, and references therein). The latter value is significantly lower than that of Fo-rich olivines from the adjacent island of Procida, which yield the highest $^3He/^4He$ ratios within the PVD (5 Ra; Piochi *et al.*, 2005; Martelli *et al.*, 2008).

SAMPLING

For this study, tephra from Vateliero and Cava Nocelle were chosen for analysis because they are among the least evolved magmas erupted at Ischia volcano. They were sampled at the type localities where the units have been recently redefined (de Vita *et al.*, 2010). The sampled volcanic rocks are either composite pumice samples or single scoria fragments. From the stratigraphic sequence of the Vateliero tephra, we collected and analyzed two composite

pumice samples representative of a basal surge bedset overlying a paleosol (sample Vat A), and a fallout deposit at the top of the stratigraphic sequence (sample Vat B). At Cava Nocelle we collected four scoria samples representative of distinct intervals in the strombolian activity. For MI studies we analyzed the stratigraphically intermediate sample (I Cn 2), which is the only one containing glassy MI.

ANALYTICAL METHODS
Sample preparation and analytical details

Samples were washed several times in deionized water, then dried and crushed to particles <1 cm in an agate mortar and sieved. Olivine and clinopyroxene phenocrysts were handpicked under a binocular microscope from crushed pumice fragments for MI studies. The selected crystals were mounted on microscope slides with an epoxy resin soluble in acetone (Crystalbond). Doubly polished sections of phenocryst-hosted MI were prepared by grinding and polishing the host minerals first with abrasive papers and then with $0.3\,\mu m$ alumina powder (water was used as lubricant). Sample thicknesses were measured via a Mitutoyo micrometer.

Analyzed MI are generally glassy or two phase (glass + shrinkage bubble), indicating a rapid quench (Lowenstern, 1994) and likely preservation of local-scale equilibrium between the trapped melt and the host mineral (Fig. 3). FTIR analyses of c. 80 MI trapped in both olivine and clinopyroxene phenocrysts were carried out at the Istituto Nazionale di Geofisica e Vulcanologia (INGV), sezione di Napoli, Osservatorio Vesuviano, using an FTIR NexusTM spectrometer from Nicolet, equipped with a heated ceramic (Globar) source, a KBr beamsplitter and an MCT detector. A high-pressure dry air (CO_2 <7 ppm) line was used to purge the system. For each spectrum 1000 scans at $4\,cm^{-1}$ were obtained. The investigated spectral domain ranges from 4000 to $650\,cm^{-1}$. H_2O and CO_2 concentrations were determined via the Beer–Lambert law (Ihinger et al., 1994). Density was estimated for each sample using the method of Lange & Carmichael (1987). The extinction coefficients used are $63.9 \pm 2\,L\,mol^{-1}cm^{-1}$ for the peak of H_2O at $3550\,cm^{-1}$, whereas for CO_2, dissolved as CO_3^{2-}, we used $308 \pm 110\,L\,mol^{-1}cm^{-1}$ for the peak at $1515\,cm^{-1}$ (Behrens et al., 2009). The latter value matches well that calculated using the empirical equation of Dixon & Pan (1995) for basalts, and is consistent with that determined for shoshonitic experimental glasses (Vetere et al., 2011). For the CO_2 absorption background correction, we subtracted from each acquisition the spectrum of a degassed glass of as similar as possible composition and thickness. The resulting spectrum was processed using the Jandel 'Peak Fit' package©.

Crystal and MI compositions including S and Cl were determined by electron microprobe. Electron microprobe
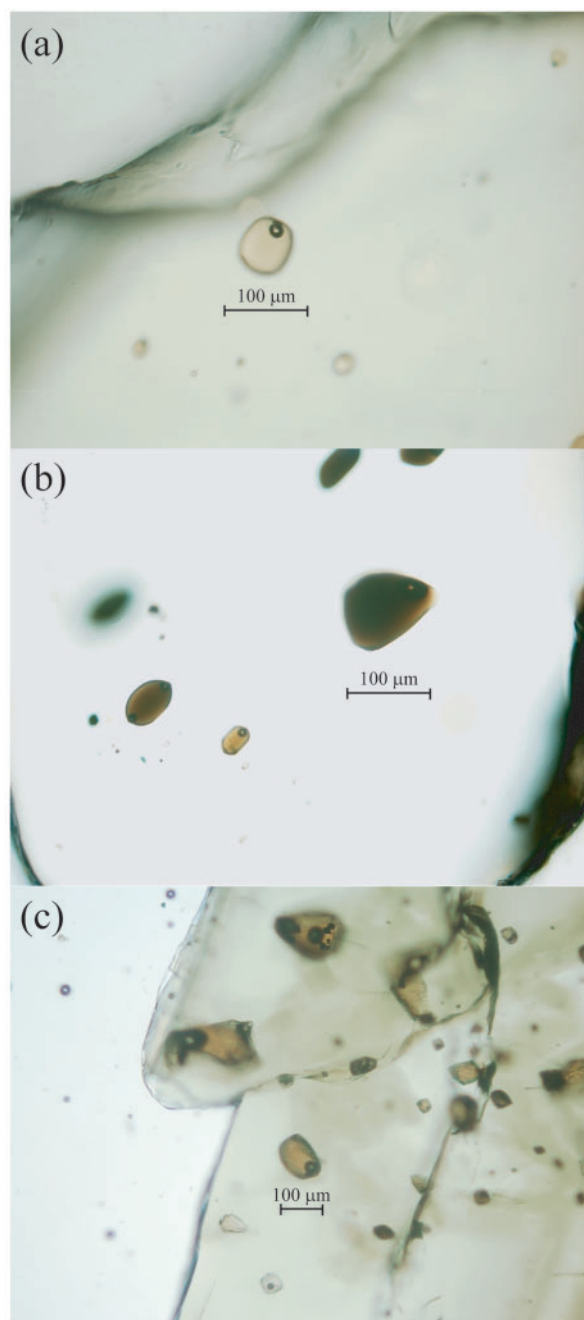
Fig. 3. Transmitted light photomicrographs of (a) Vateliero olivine-hosted MI, (b) Cava Nocelle olivine-hosted MI and (c) Vateliero pyroxene-hosted MI.

(EMP) analyses were carried out using a JEOL JXA 8200 with wavelength-dispersive spectrometry (WDS) and energy-dispersive spectrometry (EDS) combined at the INGV sezione di Roma, Italy. During the EMP-WDS analyses the operating conditions were 15 kV accelerating voltage and 7 nA probe current, providing signal stability. A probe diameter of $5\,\mu m$, with a final spot size of about

7 μm, was used to reduce alkali migration during glass analysis. The elements Na, F, Si, K, and Ca were analysed first and simultaneously. Counting time was 10 s on both peak and background; data reduction was carried out using the ZAF correction routine, provided within the JEOL software package. The following materials were used as standards for the various elements (in parentheses): (1) for glass analyses: fluorite (F), albite (Na), island basalt BIR-1 (Mg, Al, Si, Ca, Fe), orthoclase (K), sodalite (Cl), barite (Ba), nickel metal (Ni), titanium oxide (Ti), apatite (P), chromite (Cr) and spessartine (Mn); (2) for olivine analyses: forsterite (Mg, Si), pargasite, (Al, Ca,) almandine (Fe) and albite (Na). For the glass analyses, the maximum uncertainties were: 3·5% for Si, Al, Mg, Fe, Ca, K and Na; 17% for Cl and S; 24% for P, F and Cr; Ni contents were generally near or below the detection limit, implying uncertainties up to 30%. For the olivine analyses, the maximum uncertainties were: 2% for Si, Mg and Fe; 10% for Ca; near or below detection limit for Ni, Mn and Cr.

The major element compositions (oxides) of the analyzed MI are reported in Table 1, both recalculated to 100 wt % on an anhydrous basis and recalculated at 100 wt % after re-equilibration using the Petrolog3 software package (Danyushevsky & Plechov, 2011), together with the volatile species H_2O (wt %), CO_2, S and Cl (ppm). The compositions of the host olivine and pyroxene, together with the original EMPA data for MI, are reported in the Supplementary Data (available for downloading at www.http://petrology.oxfordjournals.org/).

Procedure for MI post-entrapment correction and consequences on the redox state

We used the Maurel & Maurel (1982) equation for spinel–liquid equilibrium to calculate the FeO/MgO ratio of the magma crystallizing Cr-bearing spinel and olivine in the composition range Fo_{89} to Fo_{81}. D'Antonio *et al.* (2013) provided compositional data for Cr-spinels that we assumed were in equilibrium with MI compositions representative of the melts trapped by such olivines during magmatic differentiation (I-Vat-A.1 ol3 incl1 and I-Vat-B.1 ol6, Table 1).

Because re-equilibration between the host olivine and MI appears to have been complete, as shown by the sharp boundaries between them (Fig. 4), we lack any constraints to establish the initial FeO_{tot}, unless we fix arbitrarily the oxygen fugacity and consequently compute the melt Fe^{2+}/Fe^{3+} ratio. Therefore, we assume that the measured MI FeO_{tot} values correspond to the FeO contents of a melt that equibrated with Cr-bearing spinel. Then, by adopting the FeO/MgO ratios from the melt–spinel equilibrium (from 0·875 to 1·608 for pairs involving spinels trapped within olivines ranging between Fo_{89} and Fo_{81} respectively), we determined that the maximum MgO contents

consistent with the (non-corrected) FeO_{tot} of Vat-A.1 ol3 incl1 and Vat-B ol6 MI are 6·97 and 3·58 wt % (Table 1).

We then calculated which redox conditions the Petrolog3 software package (Danyushevsky & Plechov, 2011) returned for the selected samples based on the corrected composition. As shown by D'Antonio *et al.* (2013) this occurs for Fe^{3+}/ΣFe ratios varying from 0·2 (for melts trapped in Fo_{89} olivines) to 0·3 (for melts trapped in Fo_{79} olivines), making the correction for olivine crystallization less important for the more differentiated compositions. The following linear relationship can be established between olivine molar composition and melt redox state (Fe^{3+}/ΣFe molar ratio in melt):

$$\left.\frac{Fe^{3+}}{\Sigma Fe}\right|^{melt}_{molar} = -0\cdot0081 \left.\frac{Fe}{Mg + Fe}\%\right|^{olivine}_{molar} + 0\cdot9088.$$

Corrections for all MI were made using Petrolog3, by imposing the Fe^{2+}/Fe^{3+} ratio corresponding to the above equation. The post-entrapment crystallization of the host olivine involves a fraction of 10% at most from the trapped MI.

Redox states up to Fe^{3+}/$\Sigma Fe = 0\cdot3$, corresponding to MI corrected for post-entrapment crystallization, represent an alternative scenario to that given by the nearly equivalent divalent and trivalent iron proportions. This yields redox estimates that, although more conservative than that obtained by considering the non-corrected MI, reveal that the Ischia magmas are very oxidized, exceeding the nickel–nickel oxide (NNO) buffer by more than one log unit.

RESULTS

The analyzed pumice fragments have variable vesicularity (40–60 vol. %). They are highly porphyritic and glomeroporphyritic, with 25–40 vol. % of euhedral phenocrysts and microphenocrysts of feldspar, clinopyroxene, olivine, biotite, opaque oxides and apatite, in order of decreasing abundance.

The host olivines are euhedral crystals, ∼1 mm long and characterized by Fo contents ranging from 89 to 79 mol % (Table 1). The olivine-hosted MI are glassy and usually large (up to 300 μm in length), but small inclusions are also present. In the same crystal rounded and elongated MI can coexist. They both contain one large or several small shrinkage bubbles (Fig. 3a and b). Under the petrographic microscope the MI are dark brown to light brown in colour. Their compositions (Table 1) range from K-trachybasalt to shoshonite (Fig. 2a). Tiny inclusions of dark red oxide (probably chromite) occur in a few olivine phenocrysts.

The analysed clinopyroxene phenocrysts are euhedral and vary in color from green to black. Clinopyroxene-hosted MI in samples from the Vateliero tephra have irregular shapes, with rims less sharp than those hosted in

Table 1: Original melt inclusion compositions and re-equilibrated compositions using Petrolog

	Vat A 1_ol1	Vat A 1_ol2	Vat A 1_ol3 (inc1)	Vat A 1_ol3 (inc2)	Vat A 1_ol3 (inc3)	Vat A 1_ol3 (inc4)	Vat A 1_ol4 (inc1)	Vat A 1_ol4 (inc2)	Vat A 1_ol5 (inc1)	Vat A 1_ol5 (inc2)	Vat A 1_px1
Original compositions normalized to 100% on an anhydrous basis											
SiO_2	48·63	52·45	54·74	54·46	n.a.	n.a.	52·04	n.a.	49·65	49·62	51·15
TiO_2	1·40	1·52	1·57	1·51	n.a.	n.a.	1·80	n.a.	1·81	1·90	1·10
Al_2O_3	18·19	18·72	18·63	18·61	n.a.	n.a.	17·52	n.a.	18·05	18·13	19·83
FeOt	7·75	6·25	5·57	5·51	n.a.	n.a.	6·82	n.a.	8·85	8·69	6·94
MnO	0·15	0·20	0·08	0·09	n.a.	n.a.	0·16	n.a.	0·10	0·18	0·22
MgO	4·02	3·20	2·71	2·80	n.a.	n.a.	3·66	n.a.	3·62	3·16	3·54
CaO	13·31	9·38	7·71	7·99	n.a.	n.a.	11·01	n.a.	10·27	10·70	7·56
Na_2O	2·28	3·64	4·05	3·90	n.a.	n.a.	3·63	n.a.	3·12	3·13	3·47
K_2O	3·63	3·81	4·22	4·43	n.a.	n.a.	2·60	n.a.	3·62	3·59	4·92
P_2O_5	0·64	0·83	0·74	0·70	n.a.	n.a.	0·76	n.a.	0·90	0·90	1·27
Total	100·00	100·00	100·00	100·00			100·00		100·00	100·00	100·00
Re-equilibrated compositions using Petrolog v3.1.1.2											
SiO_2	48·28	51·98	54·16	54·21	n.a.	n.a.	51·63	n.a.	49·39	49·22	
TiO_2	1·33	1·46	1·54	1·49	n.a.	n.a.	1·74	n.a.	1·78	1·85	
Al_2O_3	17·25	18·02	18·35	18·34	n.a.	n.a.	16·97	n.a.	17·78	17·63	
Fe_2O_3	1·85	1·47	1·46	1·42	n.a.	n.a.	1·67	n.a.	2·71	2·71	
FeO	6·15	4·94	4·36	4·25	n.a.	n.a.	5·33	n.a.	6·50	6·50	
MnO	0·14	0·19	0·08	0·09	n.a.	n.a.	0·15	n.a.	0·10	0·18	
MgO	6·15	4·94	3·58	3·42	n.a.	n.a.	5·07	n.a.	4·08	4·09	
CaO	12·63	9·03	7·59	7·88	n.a.	n.a.	10·66	n.a.	10·12	10·41	
Na_2O	2·17	3·50	3·98	3·84	n.a.	n.a.	3·52	n.a.	3·07	3·04	
K_2O	3·45	3·67	4·16	4·37	n.a.	n.a.	2·52	n.a.	3·57	3·49	
P_2O_5	0·60	0·80	0·73	0·69	n.a.	n.a.	0·74	n.a.	0·89	0·88	
Total	100·00	100·00	100·00	100·00	0·00	0·00	100·00	0·00	100·00	100·00	
Cl	4140	3000	2140	2220			1380		3000	2850	3660
S	1435	880	900	725			1310		1580	1565	1810
Fo (mol %)	85·8	86·1	84·0	83·7			85·0		78·5	78·5	
H_2O (wt %)	1·05	1·26	1·76	1·19	1·01	1·01	1·78	1·91	1·62	n.a.	2·02
CO_2 (ppm)	1440	622	283	176	b.d.l.	333	1167	1120	1556	n.a.	216
MI thickness (μm)	108	60	58	58	58	58	68	68	85		50
P (MPa), non-corrected MI	186·7	142·7	106·1	71·6		97·3	207·6	202·5	264·6		101·5
Depth (m), non-corrected MI	7622	5827	4337	2930		3976	8473	8268	10801		4150
P (MPa), corrected MI	186·1	127·7	92·3	55·4		70·6	206·6	188·9	273·3		71·9
Depth (m), corrected MI	7598	5217	3774	2269		2889	8434	7713	11154		2942
T from Petrolog (°C)	1052	1066	1077	1077			1062		1067	1036	

	Vat A 1_px2 (inc1)	Vat A 1_px2 (inc2)	Vat A 1_px2 (inc3)	Vat A 1_px3	Vat A 1_px4	Vat A 1_px5	Vat A 1_px6 (inc1)	Vat A 1_px6 (inc2)	Vat A 1_px6 (inc3)	Vat A ol1	Vat A ol2
Original compositions normalized to 100% on an anhydrous basis											
SiO_2	n.a.	50·13	50·05	n.a.	n.a.	n.a.	49·87	53·93	51·31	50·47	47·97
TiO_2	n.a.	1·15	1·02	n.a.	n.a.	n.a.	1·32	1·30	1·18	1·94	1·50
Al_2O_3	n.a.	19·99	19·95	n.a.	n.a.	n.a.	20·84	19·76	20·67	17·42	17·83

(continued)

Table 1: Continued

	Vat A 1__px2 (inc1)	Vat A 1__px2 (inc2)	Vat A 1__px2 (inc3)	Vat A 1__px3	Vat A 1__px4	Vat A 1__px5	Vat A 1__px6 (inc1)	Vat A 1__px6 (inc2)	Vat A 1__px6 (inc3)	Vat A ol1	Vat A ol2
FeOt	n.a.	6·89	7·57	n.a.	n.a.	n.a.	7·09	6·66	5·88	7·00	7·70
MnO	n.a.	0·16	0·17	n.a.	n.a.	n.a.	0·17	0·18	0·17	0·10	0·12
MgO	n.a.	3·99	3·04	n.a.	n.a.	n.a.	3·38	3·07	3·39	3·67	3·68
CaO	n.a.	8·06	9·05	n.a.	n.a.	n.a.	8·71	7·14	8·53	11·97	14·32
Na_2O	n.a.	3·12	3·26	n.a.	n.a.	n.a.	3·04	4·16	3·25	3·57	1·99
K_2O	n.a.	5·25	4·28	n.a.	n.a.	n.a.	4·37	3·19	4·62	3·00	4·01
P_2O_5	n.a.	1·27	1·60	n.a.	n.a.	n.a.	1·20	0·61	1·00	0·85	0·88
Total	0·00	100·00	100·00				100·00	100·00	100·00	100·00	100·00
Re-equilibrated compositions using Petrolog v3.1.1.2											
SiO_2										49·92	47·53
TiO_2										1·84	1·42
Al_2O_3										16·47	16·88
Fe_2O_3										1·58	1·82
FeO										5·59	6·08
MnO										0·09	0·11
MgO										6·16	6·09
CaO										11·33	13·56
Na_2O										3·38	1·88
K_2O										2·84	3·80
P_2O_5										0·80	0·83
Total										100·00	100·00
Cl		3830	3960				4270	1880	3870	1830	3650
S		2295	1940				2070	1825	1960	1336	1672
Fo (mol %)										87·2	85·9
H_2O (wt %)	1·72	0·82	1·67	1·69	0·91	2·01	2·02	1·83	1·63	3·64	3·17
CO_2 (ppm)	b.d.l.	168	868	b.d.l.	b.d.l.	b.d.l.	b.d.l.	b.d.l.	281	1907	2473
MI thickness (μm)	70	70	70	70	90	57	64	64	64	32	36
P (MPa), non-corrected MI		70·9	183·2						87·3	302·8	288·5
Depth (m), non-corrected MI		2900	7482						3570	12356	11774
P (MPa), corrected MI		41·1	154·8						73·8	318·3	316·2
Depth (m), corrected MI		1686	6324						3019	12989	12903
T from Petrolog (°C)										1055	1025

	Vat A ol3	Vat A ol4	Vat A ol5 (inc1)	Vat A ol5 (inc1) spot1	Vat A ol5 (inc1) spot2	Vat A ol5 (inc1) spot3	Vat A ol5 (inc1) spot4	Vat A ol5 (inc1) spot5	Vat A ol5 (inc1) spot6	Vat A ol5 (inc2)	Vat A ol6
Original compositions normalized to 100% on an anhydrous basis											
SiO_2	48·87	47·47	47·97	47·96	47·31	47·92	47·72	47·74	47·26	48·11	48·38
TiO_2	2·00	1·68	1·24	1·20	1·45	1·41	1·54	1·37	1·48	1·23	1·85
Al_2O_3	17·30	18·37	17·09	17·39	17·50	17·28	17·27	17·22	17·58	17·73	18·84
FeOt	7·01	8·67	8·03	7·98	8·03	7·85	8·18	8·21	7·99	7·59	8·01
MnO	0·13	0·24	0·14	0·14	0·16	0·15	0·17	0·19	0·09	0·15	0·15
MgO	3·96	3·77	4·23	4·34	4·22	4·25	4·00	3·80	3·46	3·98	3·32

(continued)

Table 1: Continued

	Vat A ol3	Vat A ol4	Vat A ol5 (inc1)	Vat A ol5 (inc1) spot1	Vat A ol5 (inc1) spot2	Vat A ol5 (inc1) spot3	Vat A ol5 (inc1) spot4	Vat A ol5 (inc1) spot5	Vat A ol5 (inc1) spot6	Vat A ol5 (inc2)	Vat A ol6
CaO	12·43	11·85	14·34	14·07	14·34	14·14	14·36	14·44	14·89	14·17	10·65
Na_2O	2·74	2·75	2·07	2·09	2·10	2·01	1·99	2·19	2·13	2·08	3·17
K_2O	4·06	3·79	4·10	4·07	4·12	4·16	4·07	4·05	4·32	4·19	4·39
P_2O_5	1·50	1·40	0·79	0·77	0·77	0·83	0·70	0·78	0·79	0·77	1·24
Total	100·00	100·00	100·00	100·00	100·00	100·00	100·00	100·00	100·00	100·00	100·00
Re-equilibrated compositions using Petrolog v3.1.1.2											
SiO_2	48·46	47·19	47·58	47·58	46·93	47·58	47·29	47·28	46·83	47·75	48·09
TiO_2	1·91	1·63	1·18	1·15	1·38	1·35	1·46	1·29	1·39	1·18	1·80
Al_2O_3	16·51	17·83	16·30	16·64	16·67	16·54	16·35	16·24	16·55	17·00	18·26
Fe_2O_3	1·59	2·37	1·90	1·89	1·92	1·86	1·94	1·94	1·89	1·81	2·32
FeO	5·58	6·57	6·33	6·29	6·39	6·19	6·45	6·47	6·30	5·97	6·14
MnO	0·12	0·23	0·13	0·13	0·15	0·14	0·16	0·18	0·08	0·14	0·15
MgO	6·05	4·97	6·27	6·23	6·24	6·13	6·36	6·36	6·12	5·83	4·28
CaO	11·87	11·50	13·68	13·46	13·66	13·54	13·60	13·62	14·02	13·57	10·38
Na_2O	2·61	2·67	1·97	2·00	2·00	1·92	1·88	2·06	2·01	1·99	3·09
K_2O	3·87	3·68	3·91	3·89	3·93	3·98	3·85	3·82	4·07	4·02	4·28
P_2O_5	1·43	1·36	0·75	0·74	0·73	0·79	0·66	0·74	0·74	0·74	1·21
Total	100·00	100·00	100·00	100·00	100·00	100·00	100·00	100·00	100·00	100·00	100·00
Cl	2530	3150	4070	3880	3410	3870	3310	3710	4140	3900	2960
S	2144	1868	1892	1672	1892	2020	1608	1648	1988	1784	1656
Fo (mol %)	87·0	81·8	85·8	85·8	85·8	85·8	85·8	85·8	85·8	85·6	80·9
H_2O (wt %)	2·83	3·35	2·25	2·25	2·25	2·25	2·25	2·25	2·25	2·53	2·78
CO_2 (ppm)	933	603	1837	b.d.l.	b.d.l.	b.d.l.	b.d.l.	b.d.l.	b.d.l.	1667	304
MI thickness (μm)	41	31	53	53	53	53	53	53	53	42	37
P (MPa), non-corrected MI	194·7	176·3	236·8							224·6	127·9
Depth (m), non-corrected MI	7949	7200	9666							9168	5223
P (MPa), corrected MI	190·3	171	250·6							232·7	118·3
Depth (m), corrected MI	7770	6983	10228							9498	4834
T from Petrolog (°C)	1062	1053	1057	1064	1057	1059	1044	1035	1014	1045	1051

	Vat A ol7	Vat A ol8	Vat A ol9	Vat A ol10	Vat A ol11	Vat A ol12 (inc1)	Vat A ol12 (inc2)	Vat A ol13	Vat A ol15	Vat A ol16	Vat A ol17 (inc1)
Original compositions normalized to 100% on an anhydrous basis											
SiO_2	n.a.	50·90	50·71	n.a.	n.a.	n.a.	n.a.	n.a.	50·22	51·85	51·45
TiO_2	n.a.	1·93	1·69	n.a.	n.a.	n.a.	n.a.	n.a.	1·28	1·51	1·40
Al_2O_3	n.a.	16·66	18·55	n.a.	n.a.	n.a.	n.a.	n.a.	18·45	17·71	19·83
FeOt	n.a.	6·18	7·07	n.a.	n.a.	n.a.	n.a.	n.a.	7·19	5·94	6·13
MnO	n.a.	0·21	0·14	n.a.	n.a.	n.a.	n.a.	n.a.	0·15	0·06	0·14
MgO	n.a.	4·18	3·62	n.a.	n.a.	n.a.	n.a.	n.a.	3·42	3·56	3·23
CaO	n.a.	12·00	11·30	n.a.	n.a.	n.a.	n.a.	n.a.	12·34	13·50	10·11
Na_2O	n.a.	3·38	3·63	n.a.	n.a.	n.a.	n.a.	n.a.	2·51	1·78	3·49
K_2O	n.a.	3·63	2·60	n.a.	n.a.	n.a.	n.a.	n.a.	3·79	3·20	3·57

(continued)

Table 1: Continued

	Vat A ol7	Vat A ol8	Vat A ol9	Vat A ol10	Vat A ol11	Vat A ol12 (inc1)	Vat A ol12 (inc2)	Vat A ol13	Vat A ol15	Vat A ol16	Vat A ol17 (inc1)
P_2O_5	n.a.	0·93	0·67	n.a.	n.a.	n.a.	n.a.	n.a.	0·65	0·88	0·66
Total		100·00	100·00						100·00	100·00	100·00
Re-equilibrated compositions using Petrolog v3.1.1.2											
SiO_2	n.a.	50·44	50·44	n.a.	n.a.	n.a.	n.a.	n.a.	49·82	51·27	51·06
TiO_2	n.a.	1·85	1·66	n.a.	n.a.	n.a.	n.a.	n.a.	1·23	1·43	1·36
Al_2O_3	n.a.	15·95	18·18	n.a.	n.a.	n.a.	n.a.	n.a.	17·77	16·80	19·23
Fe_2O_3	n.a.	1·34	1·84	n.a.	n.a.	n.a.	n.a.	n.a.	1·79	1·33	1·51
FeO	n.a.	4·98	5·42	n.a.	n.a.	n.a.	n.a.	n.a.	5·59	4·80	4·88
MnO	n.a.	0·20	0·14	n.a.	n.a.	n.a.	n.a.	n.a.	0·14	0·06	0·14
MgO	n.a.	6·13	4·48	n.a.	n.a.	n.a.	n.a.	n.a.	5·07	5·94	4·53
CaO	n.a.	11·49	11·07	n.a.	n.a.	n.a.	n.a.	n.a.	11·89	12·81	9·81
Na_2O	n.a.	3·24	3·56	n.a.	n.a.	n.a.	n.a.	n.a.	2·42	1·69	3·38
K_2O	n.a.	3·48	2·55	n.a.	n.a.	n.a.	n.a.	n.a.	3·65	3·04	3·46
P_2O_5	n.a.	0·89	0·66	n.a.	n.a.	n.a.	n.a.	n.a.	0·63	0·83	0·64
Total		100·00	100·00						100·00	100·00	100·00
Cl		2440	1120						3040	2280	1960
S		1904	1508						1472	1208	1072
Fo (mol %)	n.a.	88·5	83·1						84·3	87·7	85·1
H_2O (wt %)	2·66	3·41	3·44	3·07	2·91	2·04	1·96	3·07	n.a.	n.a.	3·47
CO_2 (ppm)	251	639	2830	2771	705	b.d.l.	b.d.l.	1764	n.a.	n.a.	1243
MI thickness (μm)	38	30	30	34	39	29	29	27			31
P (MPa), non-corrected MI	107·0	181·3	355·2	335·2	171·0			267·7			240·5
Depth (m), non-corrected MI	4373	7404	14495	13680	6981			10927			9817
P (MPa), corrected MI	93·8	171·6	379·3	362·7	163·1			278·8			238·5
Depth (m), corrected MI	3835	7007	15476	14799	6661			11378			9735
T from Petrolog (°C)		1084	1056						1031	1015	1053

	Vat A ol17 (inc2)	VatB ol1 (inc1)	VatB ol1 (inc2)	VatB ol2	VatB ol3	VatB ol4	VatB ol5	VatB ol6	VatB ol7	VatB ol8	VatB ol9
Original compositions normalized to 100% on an anhydrous basis											
SiO_2	n.a.	n.a.	n.a.	n.a.	n.a.	n.a.	50·44	51·86	49·66	49·72	48·64
TiO_2	n.a.	n.a.	n.a.	n.a.	n.a.	n.a.	1·60	1·49	2·20	1·33	1·95
Al_2O_3	n.a.	n.a.	n.a.	n.a.	n.a.	n.a.	18·05	16·24	18·46	18·06	18·34
FeOt	n.a.	n.a.	n.a.	n.a.	n.a.	n.a.	6·95	6·45	7·47	7·50	7·38
MnO	n.a.	n.a.	n.a.	n.a.	n.a.	n.a.	0·15	0·16	0·19	0·16	0·10
MgO	n.a.	n.a.	n.a.	n.a.	n.a.	n.a.	3·31	4·06	3·33	3·44	3·71
CaO	n.a.	n.a.	n.a.	n.a.	n.a.	n.a.	10·48	13·75	10·58	13·08	11·34
Na_2O	n.a.	n.a.	n.a.	n.a.	n.a.	n.a.	3·47	2·52	3·19	2·55	2·84
K_2O	n.a.	n.a.	n.a.	n.a.	n.a.	n.a.	4·00	2·90	3·86	3·45	4·33
P_2O_5	n.a.	n.a.	n.a.	n.a.	n.a.	n.a.	1·55	0·59	1·06	0·73	1·37
Total							100·00	100·00	100·00	100·00	100·00
Re-equilibrated compositions using Petrolog v3.1.1.2											
SiO_2	n.a.	n.a.	n.a.	n.a.	n.a.	n.a.	50·13	51·11	49·35	49·23	48·33
TiO_2	n.a.	n.a.	n.a.	n.a.	n.a.	n.a.	1·57	1·39	2·15	1·27	1·89
Al_2O_3	n.a.	n.a.	n.a.	n.a.	n.a.	n.a.	17·68	15·20	18·07	17·23	17·78

(continued)

Table 1: Continued

	Vat A ol17 (inc2)	VatB ol1 (inc1)	VatB ol1 (inc2)	VatB ol2	VatB ol3	VatB ol4	VatB ol5	VatB ol6	VatB ol7	VatB ol8	VatB ol9
Fe_2O_3	n.a.	n.a.	n.a.	n.a.	n.a.	n.a.	1·94	1·40	2·17	1·86	1·83
FeO	n.a.	n.a.	n.a.	n.a.	n.a.	n.a.	5·38	5·30	5·72	5·89	5·74
MnO	n.a.	n.a.	n.a.	n.a.	n.a.	n.a.	0·15	0·15	0·19	0·15	0·10
MgO	n.a.	n.a.	n.a.	n.a.	n.a.	n.a.	4·05	6·97	4·05	5·47	5·06
CaO	n.a.	n.a.	n.a.	n.a.	n.a.	n.a.	10·26	12·87	10·36	12·48	10·99
Na_2O	n.a.	n.a.	n.a.	n.a.	n.a.	n.a.	3·40	2·35	3·12	2·43	2·75
K_2O	n.a.	n.a.	n.a.	n.a.	n.a.	n.a.	3·92	2·71	3·78	3·29	4·20
P_2O_5	n.a.	n.a.	n.a.	n.a.	n.a.	n.a.	1·52	0·55	1·04	0·70	1·33
Total							100·00	100·00	100·00	100·00	100·00
Cl							1810	2500	1860	2770	2760
S							1212	1538·5	1464	1624	1792
Fo (mol %)							81·8	88·7	80·9	84·6	84·4
H_2O (wt %)	3·3	3·2	1·93	2·64	2·52	2·76	1·58	1·56	2·38	2·04	2·7
CO_2 (ppm)	1102	2313	1206	2053	4409	862	1708	1664	1468	1976	697
MI thickness (μm)	35	43	43	42	30	27	44	65	40	34	41
P (MPa), non-corrected MI	216·9	307·4	211·0	285·4	423·1	185·4	263·0	212·6	252·8	246·8	173·6
Depth (m), non-corrected MI	8854	12545	8614	11649	17261	7571	10733	8678	10317	10075	7090
P (MPa), corrected MI	219·0	329·0	198·7	295·5	464·0	178·2	273·4	218·8	260·1	264·5	165·3
Depth (m), corrected MI	8940	13425	8112	12059	18930	7276	11158	8932	10616	10795	6750
T from Petrolog (°C)							1054	1049	1049	1023	1062

	VatB ol10	VatB ol11	VatB ol12	VatB ol13	VatB ol14	VatB ol15	VatB ol16	Vat B ol17	Vat B ol18	I_Cn2 ol1 (inc2)	I_Cn2 ol1 (inc1)
Original compositions normalized to 100% on an anhydrous basis											
SiO_2	51·03	50·20	49·56	n.a.	n.a.	n.a.	n.a.	52·34	48·41	n.a.	n.a.
TiO_2	1·27	1·68	1·34	n.a.	n.a.	n.a.	n.a.	1·76	1·31	n.a.	n.a.
Al_2O_3	17·63	18·34	18·23	n.a.	n.a.	n.a.	n.a.	16·46	19·22	n.a.	n.a.
FeOt	6·62	6·40	6·94	n.a.	n.a.	n.a.	n.a.	6·16	7·67	n.a.	n.a.
MnO	0·18	0·10	0·08	n.a.	n.a.	n.a.	n.a.	0·11	0·13	n.a.	n.a.
MgO	3·81	3·24	3·95	n.a.	n.a.	n.a.	n.a.	3·94	3·75	n.a.	n.a.
CaO	12·83	12·84	12·87	n.a.	n.a.	n.a.	n.a.	12·75	13·00	n.a.	n.a.
Na_2O	2·61	3·03	2·61	n.a.	n.a.	n.a.	n.a.	3·36	2·39	n.a.	n.a.
K_2O	3·45	3·47	3·64	n.a.	n.a.	n.a.	n.a.	2·55	3·48	n.a.	n.a.
P_2O_5	0·57	0·70	0·77	n.a.	n.a.	n.a.	n.a.	0·58	0·64	n.a.	n.a.
Total	100·00	100·00	100·00					100·00	100·00		
Re-equilibrated compositions using Petrolog v3.1.1.2											
SiO_2	50·47	49·74	49·18	n.a.	n.a.	n.a.	n.a.	51·78	48·01	n.a.	n.a.
TiO_2	1·20	1·60	1·29	n.a.	n.a.	n.a.	n.a.	1·68	1·26	n.a.	n.a.
Al_2O_3	16·71	17·51	17·54	n.a.	n.a.	n.a.	n.a.	15·70	18·43	n.a.	n.a.
Fe_2O_3	1·48	1·47	1·62	n.a.	n.a.	n.a.	n.a.	1·36	1·92	n.a.	n.a.
FeO	5·33	5·08	5·49	n.a.	n.a.	n.a.	n.a.	4·95	6·05	n.a.	n.a.
MnO	0·17	0·10	0·08	n.a.	n.a.	n.a.	n.a.	0·10	0·12	n.a.	n.a.
MgO	6·20	5·37	5·67	n.a.	n.a.	n.a.	n.a.	6·07	5·51	n.a.	n.a.

(continued)

Table 1: Continued

	VatB ol10	VatB ol11	VatB ol12	VatB ol13	VatB ol14	VatB ol15	VatB ol16	Vat B ol17	Vat B ol18	I_Cn2 ol1 (inc2)	I_Cn2 ol1 (inc1)
CaO	12·16	12·26	12·38	n.a.	n.a.	n.a.	n.a.	12·16	12·46	n.a.	n.a.
Na_2O	2·47	2·89	2·51	n.a.	n.a.	n.a.	n.a.	3·21	2·29	n.a.	n.a.
K_2O	3·27	3·31	3·50	n.a.	n.a.	n.a.	n.a.	2·43	3·34	n.a.	n.a.
P_2O_5	0·54	0·67	0·74	n.a.	n.a.	n.a.	n.a.	0·55	0·61	n.a.	n.a.
Total	100·00	100·00	100·00					100·00	100·00		
Cl	3200	2290	2720					1800	2480		
S	1399	1328	1492					1312	1508		
Fo (mol %)	87·5	86·6	86·2					88·1	84·5		
H_2O (wt %)	2·37	2·15	3·52	1·27	2·46	2·9	1·68	1·63	4·25	1·37	1·94
CO_2 (ppm)	1716	2100	3956	b.d.l.	b.d.l.	2350	1352	1614	847	b.d.l.	b.d.l.
MI thickness (µm)	45	33	33	14	45	43	45	39	30	41	41
P (MPa), non-corrected MI	236·9	256·9	394·5			307·6	223·4	226·4	210·9		
Depth (m), non-corrected MI	9669	10484	16096			12550	9120	9242	8608		
P (MPa), corrected MI	244·7	271·3	438·0			326·0	209·3	229·8	208·3		
Depth (m), corrected MI	9988	11072	17870			13303	8544	9380	8504		
T from Petrolog (°C)	1047	1019	1055					1059	1047		

	I_Cn2 ol2	I_Cn2 ol3	I_Cn2 ol4	I_Cn2 ol5	I_Cn2 ol6	I_Cn2 ol7	I_Cn2 ol8	I_Cn2 ol9	I_Cn2 ol10 (inc1)	I_Cn3 ol10 (inc2)	I_Cn2 ol11
Original compositions normalized to 100% on an anhydrous basis											
SiO_2	n.a.	n.a.	n.a.	49·08	n.a.	50·44	49·19	n.a.	52·27	49·27	48·27
TiO_2	n.a.	n.a.	n.a.	1·23	n.a.	1·62	1·88	n.a.	1·57	1·57	1·34
Al_2O_3	n.a.	n.a.	n.a.	17·66	n.a.	18·37	16·89	n.a.	18·91	19·09	17·48
FeOt	n.a.	n.a.	n.a.	6·50	n.a.	6·91	7·77	n.a.	6·99	8·07	7·47
MnO	n.a.	n.a.	n.a.	0·07	n.a.	0·06	0·10	n.a.	0·04	0·07	0·13
MgO	n.a.	n.a.	n.a.	4·41	n.a.	3·50	4·31	n.a.	2·78	3·02	4·05
CaO	n.a.	n.a.	n.a.	14·17	n.a.	11·27	12·30	n.a.	8·89	10·85	15·04
Na_2O	n.a.	n.a.	n.a.	2·19	n.a.	3·63	2·92	n.a.	3·90	2·97	2·02
K_2O	n.a.	n.a.	n.a.	4·02	n.a.	3·50	3·25	n.a.	4·00	4·23	3·63
P_2O_5	n.a.	n.a.	n.a.	0·67	n.a.	0·72	1·39	n.a.	0·64	0·87	0·57
Total				100·00		100·00	100·00		100·00	100·00	100·00
Re-equilibrated compositions using Petrolog v3.1.1.2											
SiO_2	n.a.	n.a.	n.a.	48·65	n.a.	49·87	48·80	n.a.	51·94	48·93	47·80
TiO_2	n.a.	n.a.	n.a.	1·17	n.a.	1·53	1·81	n.a.	1·54	1·53	1·26
Al_2O_3	n.a.	n.a.	n.a.	16·81	n.a.	17·36	16·26	n.a.	18·53	18·62	16·48
Fe_2O_3	n.a.	n.a.	n.a.	1·40	n.a.	1·56	1·86	n.a.	2·07	2·42	1·68
FeO	n.a.	n.a.	n.a.	5·25	n.a.	5·51	6·10	n.a.	5·29	6·00	5·96
MnO	n.a.	n.a.	n.a.	0·07	n.a.	0·06	0·10	n.a.	0·04	0·07	0·12
MgO	n.a.	n.a.	n.a.	6·62	n.a.	6·04	5·95	n.a.	3·51	3·97	6·66
CaO	n.a.	n.a.	n.a.	13·48	n.a.	10·65	11·84	n.a.	8·71	10·58	14·18
Na_2O	n.a.	n.a.	n.a.	2·08	n.a.	3·43	2·81	n.a.	3·82	2·90	1·90
K_2O	n.a.	n.a.	n.a.	3·83	n.a.	3·31	3·13	n.a.	3·92	4·13	3·42
P_2O_5	n.a.	n.a.	n.a.	0·64	n.a.	0·68	1·34	n.a.	0·63	0·85	0·54

(continued)

Table 1: Continued

	I__Cn2 ol2	I__Cn2 ol3	I__Cn2 ol4	I__Cn2 ol5	I__Cn2 ol6	I__Cn2 ol7	I__Cn2 ol8	I__Cn2 ol9	I__Cn2 ol10 (inc1)	I__Cn3 ol10 (inc2)	I__Cn2 ol11
Total				100·00		100·00	100·00		100·00	100·00	100·00
Cl				3830		2580	1260		1500	3450	4440
S				1912		1404	1616		1092	1952	1828
Fo (mol %)				88·7		87·3	85·4		80·3	79·7	87·3
H_2O (wt %)	1·82	1·97	3·15	3·63	3·66	2·7	3·13	3·69	2·05	n.a.	2·35
CO_2 (ppm)	b.d.l.	b.d.l.	3435	3421	3832	1949	483	3818	b.d.l.	n.a.	2298
MI thickness (μm)	27	30	38	34	33	41	36	34	44	44	40
P (MPa), non-corrected MI			373·8	352·1	397·3	286·9	157·9	397·0			308·9
Depth (m), non-corrected MI			15250	14368	16209	11709	6447	16196			12607
P (MPa), corrected MI			412·3	389·8	447·8	304·7	146·6	447·4			271·5
Depth (m), corrected MI			16822	15904	18269	12434	5988	18253			11081
T from Petrolog (°C)				1068		1057	1077		1053	1029	1039

	I__Cn2 ol12 (inc1)	I__Cn2 ol12 (inc2)	I__Cn2 ol12 (inc3)	Vat A ol2 (inc)	Vat A ol3 (inc2)	Vat A ol3 (inc1)	Vat A ol4 (inc1)	Vat A ol4 (inc2)	Vat A ol4 (inc3)	Vat A ol6 (inc1)	Vat A ol6 (inc3)
Original compositions normalized to 100% on an anhydrous basis											
SiO_2	48·54	n.a.	n.a.	48·75	48·88	47·02	47·74	47·62	47·12	48·90	49·18
TiO_2	1·28	n.a.	n.a.	1·55	1·91	1·69	1·62	1·60	1·67	1·31	1·63
Al_2O_3	17·76	n.a.	n.a.	18·17	18·09	18·50	18·89	19·15	18·93	18·07	17·92
FeOt	7·37	n.a.	n.a.	6·82	8·47	9·25	8·58	8·42	8·66	7·37	6·95
MnO	0·18	n.a.	n.a.	0·15	0·17	0·19	0·18	0·18	0·17	0·13	0·14
MgO	3·81	n.a.	n.a.	3·59	3·21	3·52	3·07	3·40	3·39	3·67	3·14
CaO	14·37	n.a.	n.a.	13·43	10·48	11·87	11·97	11·00	11·69	13·81	12·90
Na_2O	2·13	n.a.	n.a.	2·27	3·03	2·53	2·74	2·86	2·81	2·35	2·72
K_2O	4·00	n.a.	n.a.	4·08	4·48	4·18	4·34	4·49	4·26	3·73	4·15
P_2O_5	0·55	n.a.	n.a.	1·19	1·29	1·26	0·88	1·26	1·29	0·66	1·27
Total	100·00			100·00	100·00	100·00	100·00	100·00	100·00	100·00	100·00
Re-equilibrated compositions using Petrolog v3.1.1.2											
SiO_2	47·99	n.a.	n.a.	48·30	48·57	46·73	47·39	47·31	46·83	48·40	48·66
TiO_2	1·20	n.a.	n.a.	1·47	1·86	1·64	1·56	1·55	1·62	1·23	1·54
Al_2O_3	16·62	n.a.	n.a.	17·22	17·63	17·96	18·21	18·57	18·35	17·02	16·88
Fe_2O_3	1·67	n.a.	n.a.	1·55	2·46	2·69	2·40	2·38	2·41	1·69	1·60
FeO	5·95	n.a.	n.a.	5·43	6·27	6·84	6·44	6·41	6·51	5·86	5·51
MnO	0·17	n.a.	n.a.	0·14	0·17	0·18	0·17	0·17	0·16	0·12	0·13
MgO	6·70	n.a.	n.a.	6·01	4·24	4·69	4·62	4·61	4·69	6·32	5·86
CaO	13·45	n.a.	n.a.	12·73	10·21	11·53	11·54	10·66	11·33	13·02	12·15
Na_2O	2·00	n.a.	n.a.	2·15	2·96	2·46	2·64	2·77	2·72	2·21	2·56
K_2O	3·74	n.a.	n.a.	3·87	4·37	4·06	4·18	4·35	4·13	3·51	3·91
P_2O_5	0·51	n.a.	n.a.	1·13	1·26	1·22	0·85	1·22	1·25	0·62	1·20
Total	100·00			100·00	100·00	100·00	100·00	100·00	100·00	100·00	100·00
Cl	3900			3166·67	3010·00	3280	3710·00	3510·00	3236·67	3613·33	2733·33
S	1972			2156·67	2111·67	2707·5	2020·00	2031·67	1976·67	2270·00	2236·67
Fo (mol %)	87·4		90·7	87·1	80·2	80·2	81·2	81·3	81·3	86·8	86·7

(continued)

Table 1: Continued

	I_Cn2 ol12 (inc1)	I_Cn2 ol12 (inc2)	I_Cn2 ol12 (inc3)	Vat A ol2 (inc)	Vat A ol3 (inc2)	Vat A ol3 (inc1)	Vat A ol4 (inc1)	Vat A ol4 (inc2)	Vat A ol4 (inc3)	Vat A ol6 (inc1)	Vat A ol6 (inc3)
H_2O (wt %)	1·84	2·47	2·49	3·33	2·33	2·33	2·51	1·90	1·28	3·43	3·65
CO_2 (ppm)	2112	4462	4601	2632·28	882	294	b.d.l.	b.d.l.	b.d.l.	2872	1058
MI thickness (μm)	47	47	47	32	36	36	33	33	33	35	35
P (MPa), non-corrected MI	225·4	368·8	432·4	309·1	207·3	113·7				322·4	217·9
Depth (m), non-corrected MI	9200	15047	15049	12615	8464	4645				13157	8896
P (MPa), corrected MI	252·99	467·9	476·7	334·60	206·8	107·8				355·4	219·2
Depth (m), corrected MI	10326	19089	19448	13653	8442	4406				14502	8948
T from Petrolog (°C)	1034			1028	1046	1040	1018	1048	1038	1031	1012

	Vat A ol6 (inc2)	Vat A ol7 (inc)	Vat A ol7 glass	Vat A ol8 (inc1)	Vat A ol8 (inc2)	Vat A ol9	Vat A ol10	Vat A ol11	Vat A ol14	Vat B2 ol1
Original compositions normalized to 100% on an anhydrous basis										
SiO_2	48·61	50·61	49·39	48·79	49·08	47·62	48·18	50·63	49·51	47·47
TiO_2	1·40	1·34	1·20	1·61	1·49	1·32	1·91	2·11	1·66	1·51
Al_2O_3	18·20	17·30	18·40	18·14	17·55	18·91	18·29	18·48	18·51	17·05
FeOt	7·25	6·48	7·66	6·54	6·84	7·66	8·28	7·18	7·86	7·98
MnO	0·15	0·15	0·18	0·11	0·12	0·16	0·15	0·10	0·14	0·09
MgO	3·38	3·65	3·86	3·07	3·50	3·80	3·22	2·98	3·85	3·99
CaO	14·11	13·83	11·87	14·33	14·18	13·90	11·49	9·62	10·41	15·20
Na_2O	2·38	2·77	2·77	2·56	2·43	2·04	2·98	4·04	3·05	2·14
K_2O	3·88	3·35	3·96	3·92	3·91	3·87	4·17	3·69	4·17	3·84
P_2O_5	0·64	0·51	0·72	0·92	0·89	0·72	1·33	1·16	0·84	0·74
Total	100·00	100·00	100·00	100·00	100·00	100·00	100·00	100·00	100·00	100·00
Re-equilibrated compositions using Petrolog v3.1.1.2										
SiO_2	48·11	50·17	48·82	48·30	48·56	47·22	47·82	50·34	49·23	47·03
TiO_2	1·32	1·28	1·13	1·51	1·40	1·26	1·84	2·06	1·63	1·42
Al_2O_3	17·13	16·58	17·30	17·06	16·51	18·02	17·64	18·06	18·14	16·04
Fe_2O_3	1·67	1·49	1·75	1·46	1·53	1·87	2·29	1·95	2·15	1·83
FeO	5·76	5·15	6·09	5·23	5·47	6·09	6·31	5·43	6·04	6·34
MnO	0·14	0·14	0·17	0·10	0·11	0·15	0·14	0·10	0·14	0·08
MgO	6·11	5·57	6·58	5·90	6·28	5·83	4·69	3·98	4·58	6·64
CaO	13·27	13·26	11·16	13·47	13·33	13·24	11·08	9·39	10·19	14·30
Na_2O	2·24	2·66	2·60	2·41	2·29	1·94	2·88	3·95	2·99	2·01
K_2O	3·65	3·21	3·72	3·69	3·68	3·69	4·03	3·61	4·09	3·61
P_2O_5	0·60	0·49	0·68	0·87	0·84	0·69	1·28	1·13	0·82	0·70
Total	100·00	100·00	100·00	100·00	100·00	100·00	100·00	100·00	100·00	100·00
Cl	3975·00	2440·00	4570	3590·00	3766·67	3873·33	2696·67	1613·33	3507·50	4403·33
S	2240·00	1288·33	1840	2357·50	2166·67	2361·67	2071·67	1853·33	2040·00	1968·33
Fo (mol %)	86·7	86·7	86·9	87·5	87·6	85·3	81·7	81·9	82·1	86·7
H_2O (wt %)	3·79	3·21	4·34	2·73	2·98	2·20	3·33	2·04	3·88	1·88
CO_2 (ppm)	3159	2419	567	4489	2982	2354	814	1111	2014	1725
MI thickness (μm)	35	35	35	33	33	38	39	30	31	46
P (MPa), non-corrected MI	342·5	295·7	198·8	378·4	317·0	250·7	204·5	227·3	327·2	189·5

(continued)

Table 1: Continued

	Vat A ol6 (inc2)	Vat A ol7 (inc)	Vat A ol7 glass	Vat A ol8 (inc1)	Vat A ol8 (inc2)	Vat A ol9	Vat A ol10	Vat A ol11	Vat A ol14	Vat B2 ol1
Depth (m), non-corrected MI	13976	12069	8115	15441	12936	10231	8347	9280	13354	7739
P (MPa), corrected MI	379·6	316·0	191·4	440·2	352·9	270·0	202·9	228·1	340·2	224·6
Depth (m), corrected MI	15488	12895	7814	17959	14400	11019	8283	9311	13882	9168
T from Petrolog (°C)	1013	1032	1063	993	1020	1034	1032	1050	1082	1039

	Vat B2 ol2	Vat B2 ol3	Vat B2 ol4
Original compositions normalized to 100% on an anhydrous basis			
SiO_2	49·16	49·49	46·71
TiO_2	1·60	1·24	2·05
Al_2O_3	18·61	19·37	19·96
FeOt	8·27	7·18	7·75
MnO	0·18	0·10	0·15
MgO	3·25	3·25	3·10
CaO	10·78	12·23	13·21
Na_2O	3·01	2·45	2·79
K_2O	4·12	3·94	3·32
P_2O_5	1·02	0·74	0·95
Total	100·00	100·00	100·00
Re-equilibrated compositions using Petrolog v3.1.1.2			
SiO_2	48·82	49·16	46·35
TiO_2	1·56	1·20	1·95
Al_2O_3	18·13	18·81	18·94
Fe_2O_3	2·46	1·91	1·92
FeO	6·20	5·53	6·07
MnO	0·18	0·10	0·14
MgO	4·19	4·49	5·40
CaO	10·50	11·87	12·54
Na_2O	2·93	2·38	2·65
K_2O	4·01	3·83	3·15
P_2O_5	0·99	0·72	0·90
Total	99·97	100·00	100·01
Cl	3010·00	3393·33	1780·00
S	2061·67	2113·33	1223·33
Fo (mol %)	80·0	82·7	84·6
H_2O (wt %)	2·87	2·67	1·78
CO_2 (ppm)	1688	2177	1042
MI thickness (µm)	42	35	33
P (MPa), non-corrected MI	278·9	254·0	155·3
Depth (m), non-corrected MI	11381	10366	6344
P (MPa), corrected MI	291·5	286·0	155·0
Depth (m), corrected MI	11896	11672	6330
T from Petrolog (°C)	1042	1021	1000
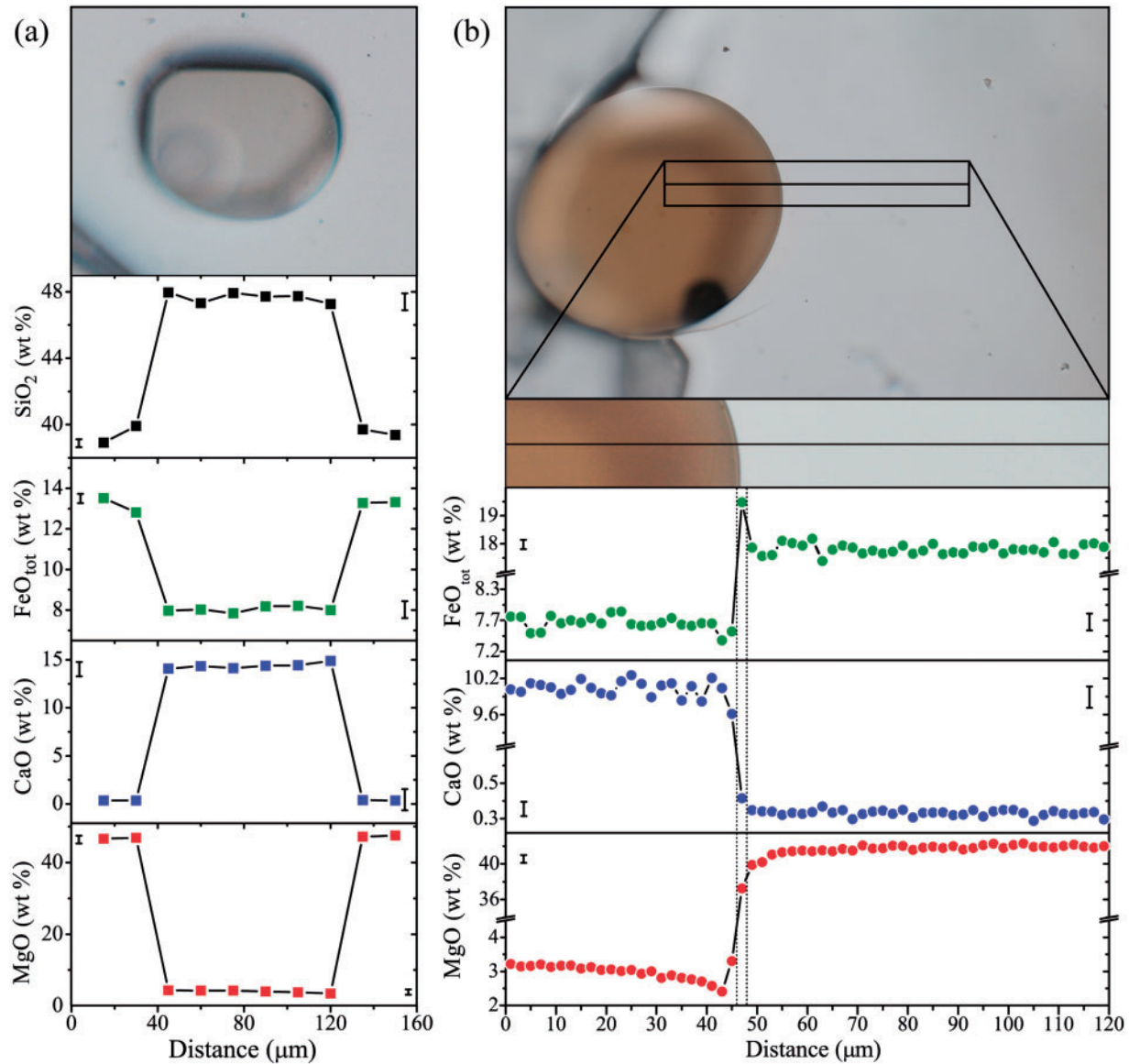
Fig. 4. (a) Variations of SiO_2, FeO_{tot}, CaO and MgO (wt %) across host olivine (sample Vat A, olivine 5; Supplementary Data) and entrapped melt inclusion (Table 1). The abrupt transitions suggest that no appreciable re-equilibration has occurred. (b) Transect of ∼120 μm at 2 μm intervals (60 points) through the MI–olivine boundary, showing abrupt chemical variations (FeO_{tot}, CaO and MgO), but also a narrow, 2–3 μm thick, transition zone in which FeO_{tot} and MgO contents are higher and lower, respectively, than in the surrounding olivine. The size of error bars is related to analytical uncertainties reported in the text.

olivine, and lengths varying up to 200 μm. The analysed MI are shoshonitic and phono-tephritic in composition (Fig. 2a); these coexist with large oxide crystals (Fig. 3c). The host clinopyroxene phenocrysts, 1–1·5 mm long, are diopsidic in composition [$Ca_{46–48}$, $Mg_{41–47}$, (Fe^{3+}, Fe^{2+}, $Mn)_{6–11}$] (see Supplementary Data).

The analyzed MI, hosted either in olivine or in clinopyroxene phenocrysts, are less evolved than either the whole-rocks, classified mostly as latite, or the residual glasses (Fig. 2a). They are compositionally similar to MI

hosted in the least differentiated Minopoli and Fondo Riccio products from CF, and Solchiaro products from Procida (Fig. 2b); they also partially overlap with the less alkaline MI from SV magmas (Fig. 2c).

No compositional variations were observed between an host olivine phenocryst and its entrapped melt inclusion (Fig. 4a; Table 1).

An additional transect of ∼120 μm at 2 μm interval (60 points, accelerating voltage 15 kV; dwell time 10 s; probe current 1·4 × 10⁻⁸ A) through the MI–olivine boundary

(Fig. 4b) shows abrupt chemical variations, but also a narrow, 2–3 μm thick, transition zone in which FeO_{tot} and MgO contents are higher and lower, respectively, than in the surrounding olivine. Moreover, the concentration profile of CaO, the diffusion of which is much slower than that of MgO and FeO (Danyushevsky et al., 2003), does not display any intermediate value at the olivine–MI boundary. These features can be ascribed either to post-entrapment crystallization on the olivine wall or to the position of the probe crystals (TAPH for Mg, PETJ for Ca and LIFH for Fe) relative to the surface of the MI at its edge, which cannot be horizontal when approaching the boundary with olivine, because of the different abrasion of olivine and MI during sample preparation. Because we cannot definitely establish that the measured compositions record the original MI–host crystal equilibrium, we discuss below results for two scenarios (non-equilibrated and re-equilibrated MI). We then consider either that their measured compositions record the original MI–host crystal equilibrium, or that complete re-equilibration took place during magma evolution, with the post-entrapment formation of a very thin crystalline layer along the MI rim (Gaetani & Watson, 2000).

FTIR spectra of the analyzed MI show water and in most cases carbonate peaks. The detected H_2O and CO_2 contents range from 0·9 to 4·3 wt % and from 170 to 4,600 ppm, respectively, and decrease with decreasing CaO content (Table 1).

MI geochemical data (Table 1) show that with decreasing CaO (used as a differentiation index), SiO_2, K_2O and Na_2O increase, whereas TiO_2 and FeO_{tot} decrease, in agreement with the general differentiation trend of the eruptive products from Ischia (Civetta et al., 1991) and the other volcanic centres of the PVD (e.g. D'Antonio et al., 1999b; Tonarini et al., 2009; Arienzo et al., 2010; Di Vito et al., 2011). CaO/Al_2O_3 ratios and MgO both decrease slightly, testifying to contemporaneous crystallization of olivine and Mg-rich pyroxene. However, MgO only decreases from 4 to 3 wt %, with a mean value of ~3·6 wt % (Fig. 5a), whereas CaO spans the entire range displayed by the Neapolitan volcanoes, thus suggesting buffering of MgO values during magmatic differentiation. The low MgO content is rather unusual considering the highly forsteritic composition of the host olivines (as high as 89 mol %; Table 1). Within the same CaO interval the other PVD volcanic rocks are characterized by MgO values from 4 to
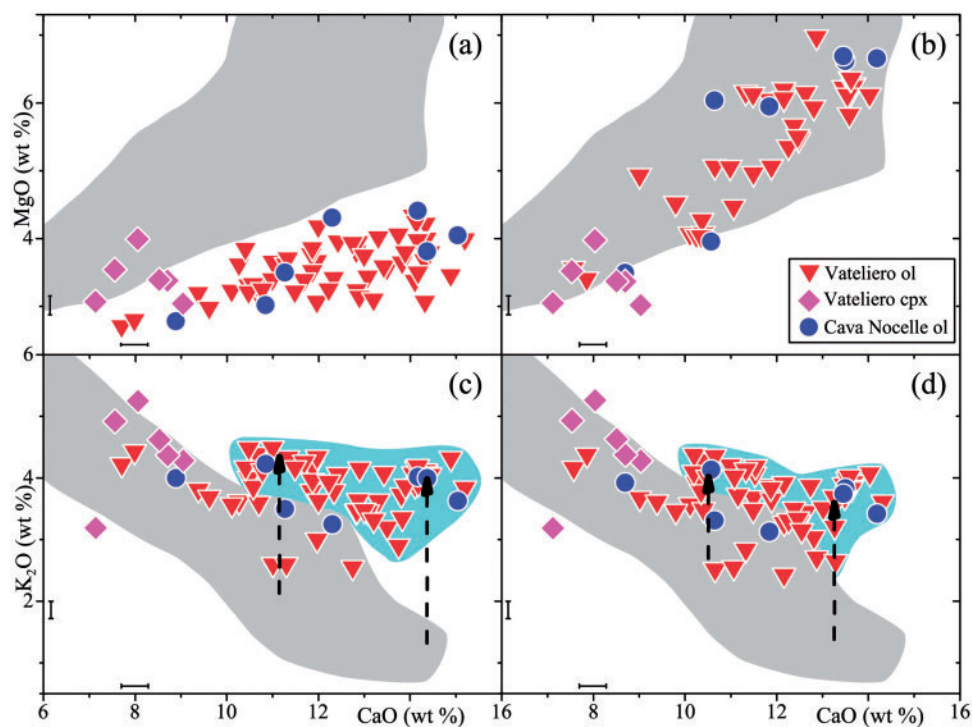
Fig. 5. (a) MgO and CaO covariation in Ischia MI compared with the trend of magmatic differentiation at Neapolitan volcanoes (original data). The Ischia MI display a nearly constant MgO value around 3·6 wt %, suggesting MgO buffering during progressive fractional crystallization. The gray field delimits the range of PVD whole-rocks and glassy groundmass from Procida samples, based on data from the literature (D'Antonio et al. 1999a, 2007; De Astis et al., 2004; Mormone et al., 2011). (b) MgO and CaO covariation for re-equilibrated MI compositions. The MI data overlap the PVD compositional field, with MgO contents spanning a wide range of values. (c) Covariation of K_2O and CaO. The light grey field delimits the data points that have K_2O and CaO contents plotting outside the PVD compositional field. Arrows indicate processes that may have occurred in addition to crystallization, such as fluid fluxing. (d) As (c), but showing re-equilibrated MI data. The size of error bars is related to analytical uncertainties reported in the text.

l0 wt % (Severs, 2007; Mangiacapra *et al.*, 2008; Mormone *et al.*, 20ll; Esposito *et al.*, 20ll; Fig. 5a). Although at Ischia primitive magmatic rocks are absent, K-basaltic lithic blocks with MgO contents up to l0 wt % occur in the adjacent island of Procida (D'Antonio *et al.*, 1999*a*, 2007; Fig. 2b). Therefore, the Ischia olivines may have equilibrated in a magma more mafic than that trapped in the MI, as suggested by sparse kink-banding and chromium-rich spinel inclusions (D'Antonio *et al.*, 20l3). Because we lack constraints on the initial FeO_{tot} of the trapped magma in the MI, unless arbitrarily imposing the oxygen fugacity, hence the melt Fe^{2+}/Fe^{3+} ratio, we applied the Maurel & Maurel (1982) equation to estimate the MgO/FeO ratio theoretically by characterizing the parental liquid coexisting with Cr-spinels prior to post-entrapment olivine crystallization. Subsequent application of the PETROLOG3 code (Danyushevsky & Plechov, 20ll), using the inferred Fe^{2+}/Fe^{3+} ratio, allows the effect of post-entrapment olivine crystallization on the MI composition to be computed by adding olivine back into the glass composition until a liquid in equilibrium with the Fo content of the host-olivine phenocryst is obtained (D'Antonio *et al.*, 20l3). The CaO vs MgO covariation in the re-equilibrated MI compositions displays a trend in good agreement with that of the PVD magmas, with the highest

values matching the field of Procida glassy groundmasses (Fig. 5b).

In Fig. 5c and d the variation of CaO vs K_2O is illustrated for the non re-equilibrated and the re-equilibrated MI compositions, respectively. In both cases K_2O contents increase with decreasing CaO. However, the data do not define a coherent trend ascribable to magmatic differentiation alone. The variability largely exceeds the analytical error and thus suggests K- and, to a lesser extent, Ca-enrichment. The CaO vs K_2O covariation of the re-equilibrated MI compositions (Fig. 5d) is little affected by post-entrapment crystallization of olivine, in agreement with microprobe profiles (Fig. 4). If we assume that post-entrapment crystallizazion affected only the CaO and K_2O contents, back-projecting the MI data into the PVD field would require crystallization of the trapped melt exceeding 20%, under extremely reduced and unrealistic redox conditions that are characterized by the absence of trivalent iron. Therefore, the large variability displayed by these two oxides needs to be explained by additional processes.

Figure 6a shows a positive correlation between K_2O and Cl in the MI. On the other hand, no clear correlation is observed between CaO and Cl (Fig. 6b), similar to the CaO vs K_2O covariation (Fig. 5c and d). Figure 6c and d illustrates the covariation of K_2O and CaO with the
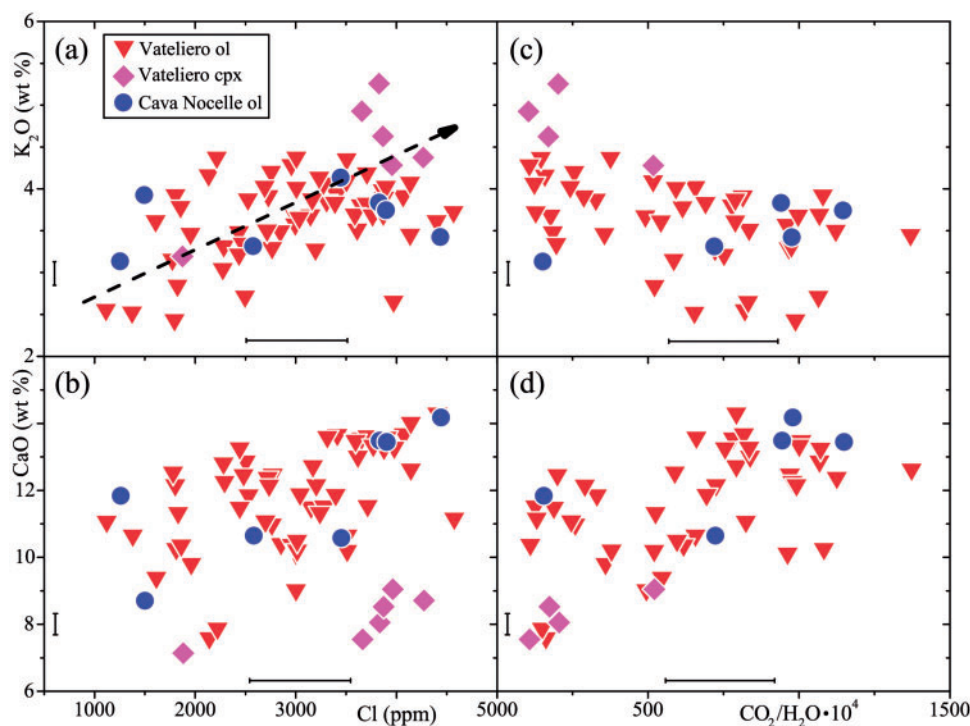
Fig. 6. CaO and K_2O variations (wt %) in MI (in the K-trachybasalt–shoshonite compositional range) vs Cl content (ppm) (a, b) and $CO_2/H_2O \times 10000$ melt ratio (c, d). Fluid-phase transfer of Cl and K, owing to fluxing of a CO_2-rich gas phase, determines enrichments in K and Cl (and in Ca to a lesser extent) overlapping the trend of fractional crystallization (see text for details). The size of error bars is related to analytical uncertainties reported in the text.

CO_2/H_2O ($\times$ 10 000) melt ratio. Whereas CaO and CO_2/H_2O ($\times$ 10 000) both decrease with differentiation, K_2O is not clearly correlated with CO_2/H_2O. The lack of significant correlations suggests that magma evolution towards low-pressure conditions (i.e. decreasing CO_2/H_2O) was not accompanied by a unique trend of degassing and fractional crystallization. Rather, variable events of CO_2-rich fluid infiltration (CO_2-fluxing) may have occurred during magmatic differentiation. This is highlighted by the Cava Nocelle MI data, which show a decrease in K_2O, CaO, CO_2/H_2O ratio and Cl contents with depressurization.

The variation of H_2O and CO_2 contents in MI is compared with computed saturation isobars at 100, 200, 300, 400 and 500 MPa in Fig. 7 for an average trachybasaltic composition. Calculations assume the non-ideal, composition-dependent model of Papale et al. (2006). The isobars were computed at 1393 K, by analogy with the shoshonites studied by Cannatelli et al. (2007) and Mangiacapra et al. (2008). Computation of the saturation surfaces is appreciably affected by the relative FeO and Fe_2O_3 proportions in the melt and was carried out consistently with $Fe^{2+}/Fe^{3+}=1$. The crude approximation of measured FeO_{tot} equal to divalent iron oxide gives Fe–Mg distribution coefficients (K_D) between MI and host olivines that are too low ($K_D \sim 0.16$ on average). Olivine–melt K_D should be around 0.3 (Roeder & Emslie, 1970) for these compositions. K_D values of ~ 0.3 for all the studied

MI and coexisting olivines are achieved only by setting $Fe^{2+}/Fe^{3+}=1$ (Table 1). This corresponds to very high oxidation states (ΔNNO $\sim$2–3; the higher the equilibration pressure and water content, the higher the oxidation state), based on the approach of Moretti & Papale (2004) and Moretti (2005). Errors (not shown in Fig. 7 for the sake of clarity) correspond to the saturation model uncertainty (Papale et al., 2006), and are $\sim$15% for H_2O and $\sim$20% for CO_2. A background degassing path (Path 1 in Fig. 7) bounding H_2O–CO_2 pairs towards the H_2O-rich side has been determined, as for the Agnano–Monte Spina, Minopoli 2 and Fondo Riccio eruptions at CF (Mangiacapra et al., 2008; Arienzo et al., 2010). Path 1 is characterized by total water (H_2O^{tot}) and carbon dioxide (CO_2^{tot}) contents of 4·25 wt % (corresponding to the highest measured water contents) and 2·1 wt %, respectively. The former is higher than, whereas the latter is similar to, the values characterizing the CF MI. The bounding degassing path towards the H_2O-poor side (Path 2 in Fig. 7) is representative of a gas-buffered system with a constant CO_2^{gas}/H_2O^{gas} ratio of five (molar).

Entrapment pressures calculated for the H_2O–CO_2 pairs vary from 70 to 430 MPa (from 40 to 480 MPa for the re-equilibrated dataset), and correspond to depths between 2·8 and 17·2 km (1·7 and 19·5 km for the re-equilibrated dataset) (Fig. 8), using an average crustal density of 2·500 kg m^{-3} (P. Capuano, personal
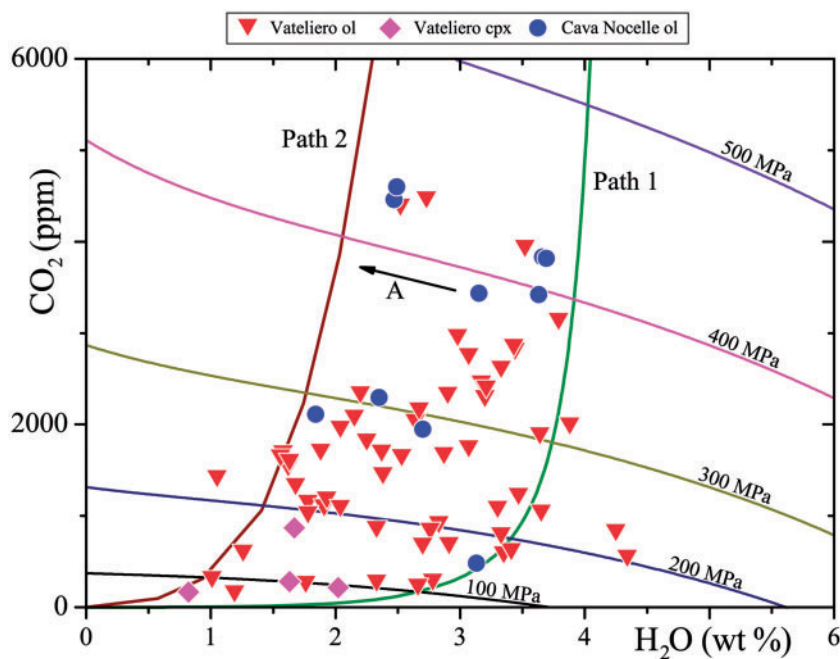
Fig. 7. Variation of H_2O vs CO_2 in MI compared with the degassing trends (Paths 1 and 2) from the Papale et al. (2006) model. Isobars are plotted for trachybasaltic composition; computation was performed at 1393 K. The background degassing Path 1, bounding the H_2O–CO_2 MI pairs towards the H_2O-rich side, is characterized by total water (H_2O^{tot}) and carbon dioxide (CO_2^{tot}) contents of 4·25 wt % and 2·1 wt %, respectively. Path 2, towards the H_2O-poor side, is that of a gas-buffered system (along the direction indicated by arrow A) with a constant CO_2^{gas}/H_2O^{gas} ratio of five (molar). Error bars (not shown) are 15% for H_2O and 23% for CO_2.

communication). For the investigated eruptions, a vertically extended magmatic plumbing system emerges with possibly a major crystallization or storage region at ~200 MPa, according to the data clustering.

DISCUSSION

The MI data obtained as part of this study can be used to investigate the physico-chemical conditions of magmatic differentiation in the presence of fluid transfer and infiltration. Mixing or mingling processes of variably evolved magma batches are an additional factor that might also contribute to the observed variations. However, mixing or mingling processes would mirror the variations of major oxides caused by fractional crystallization and would not explain the large scatter displayed, for instance, in the CaO vs K_2O (Fig. 5c and d), Cl vs K_2O and Cl vs CaO plots (Fig. 6a and b) and CO_2/H_2O ($\times$ 10 000) vs K_2O (Fig. 6c).

Alternatively, different alkali-rich magma components could be involved in the genesis of the deep parental magma. However, in the PVD alkalinity and silica-undersaturation degrees do not show significant time variations (e.g. D'Antonio *et al.*, 1999*a*, 1999*b*, 2007, 2013; De Astis *et al.*, 2004), corroborating the hypothesis of geochemically similar parental magmas, which may have been modified *en route* to the surface (see below). Because

these magmas stagnated at mid-crustal levels, where they differentiated and were partly contaminated, presumably by the local Hercynian continental crust (Pappalardo *et al.*, 2002; Tonarini *et al.*, 2004; D'Antonio *et al.*, 2007; Di Renzo *et al.*, 2011, and references therein), small compositional differences can be ascribed to crustal contamination by *c.* 2 wt % of a granodioritic crust. Nevertheless, the resulting compositional changes are too small to explain the large scatter in K_2O vs CaO (Fig. 5c and d).

Consistent with recent findings (Rust *et al.*, 2004; Spilliaert *et al.*, 2006; Mangiacapra *et al.*, 2008; Vigoroux *et al.*, 2008; Barsanti *et al.*, 2009; Aiuppa *et al.*, 2010; Arienzo *et al.*, 2010; Edmonds *et al.*, 2010; Oppenheimer *et al.*, 2011) we discuss below how the Ischia MI data highlight the role played by fluid percolation through the magmatic feeding system (i.e. fluxing), causing dehydration, CO_2 enrichment, high gas/melt ratios in the fluxed magma, and selective enrichment in elements such as the halogens and potassium (Collins *et al.*, 2009; Ferlito & Lanzafame, 2010).

Furthermore, our results allow exploration of the interplay between tectonic structures and ascending deep slab fluids to the Campanian Plain volcanoes, where the presence of CO_2 in magmas is well documented through analyses of MI in phenocrysts from (1) Procida K-trachybasalts (Esposito *et al.*, 2011; Mormone *et al.*, 2011), (2) CF shoshonitic to latitic Minopoli 2 and Fondo
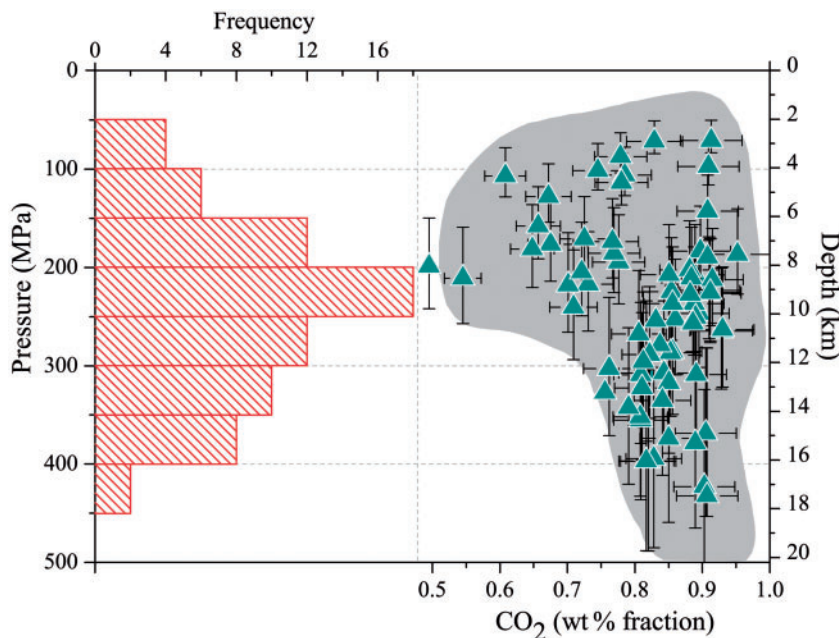
Fig. 8. Pressure and equivalent depth vs gas composition for the analyzed MI. H_2O–CO_2 pairs in MI suggest a nearly continuous 18–3 km depth range for crystallization and degassing (original data). The Gaussian distribution of crystallization depths throughout the plumbing system, with a mode between 200 and 250 MPa, is related to a main magma crystallization depth at 8–10 km, in agreement with observations at Campi Flegrei. In such an interval magmas stagnate and differentiate, as shown by the CO_2 gas proportion decreasing down to 50 wt %. The grey shaded field encompasses the pressure–depth and CO_2 gas proportion calculated by using the composition of the re-equilibrated MI and slightly expands the pressure–depth range of the original data. The size of error bars is related to model uncertainties reported in the text.

Riccio, and trachytic Agnano–Monte Spina products (Mangiacapra *et al.*, 2008; Arienzo *et al.*, 2010), and (3) tephri-phonolites of the post AD 1631 activity of Vesuvius (Marianelli *et al.*, 1999). Our results, together with these data, show that magmatic degassing in the Campanian Plain takes place at significant depths.

Physico-chemical aspects

Chemical variability and fluid transfer

Because a significant role for mixing between initially different magmas can be discarded, the upper limit of the CaO vs K_2O variation is probably due to a process of K (and to some extent Ca) enrichment (Fig. 5c and d) superimposed upon a fractional crystallization process (roughly coincident with the gray field in Fig. 5). Figure 6a shows a positive correlation between K_2O and dissolved Cl, varying from an initial $K_2O = 2.5$ wt % and $Cl_{melt} = 1000$ ppm, up to ∼4·5 wt % and ∼4500 ppm. The data are significantly scattered and do not plot along a well-defined or unique trend of differentiation (dashed line in Fig. 6a is shown for qualitative purposes only). This reflects anomalous enrichments not related to fractional crystallization but determined by the transfer of a halogen-rich, alkali-bearing gas phase, as suggested for Mt. Etna (Ferlito & Lanzafame, 2010) and Procida (Mormone *et al.*, 2011). On the other hand, the lack of correlation between CaO and Cl (Fig. 6b) suggests that differentiation (i.e. CaO decrease) is not accompanied by a simple increase in Cl content.

When crystallization is coupled to degassing, a magma rising along a single ascent path should display decreasing CO_2/H_2O, with concomitant increase in incompatible element concentrations, such as K (prior to alkali-feldspar crystallization), and decrease in CaO. Despite the generally negative correlation between CaO and CO_2/H_2O (Fig. 6d), the positive correlation between K_2O and Cl (Fig. 6a) and the lack of any correlation between CaO and Cl (Fig. 6b), as well as between CO_2/H_2O and K_2O (Fig. 6c), strengthen the hypothesis that infiltration by fluids rising from great depth (CO_2-fluxing) leads to K_2O and Cl enrichment. This process is compatible with the high total amount of volatiles ($\approx H_2O^{tot} + CO_2^{tot}$) in the Ischia parental magmas (∼6 wt %), which, in turn, is consistent with previous estimates for the volcanism of Southern Italy (Scaillet & Pichavant, 2005).

The infiltration process, which is well exemplified by the Cava Nocelle MI data (see the positive correlation between CO_2/H_2O and K_2O; Fig. 6c), strongly controls the measured K_2O variability, superimposed on the normal trend of fractional crystallization.

Gas fluxing controls the observed K enrichment by stripping K from the melt to the gas phase as KCl. By considering KCl and HCl as the most important gas species, the following chemical reactions can be written:

$$HCl_{gas} + 1/2K_2O_{melt} \leftrightarrow KCl_{melt} + 1/2H_2O_{gas} \qquad (1)$$
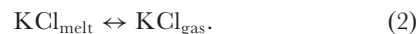
$$KCl_{melt} \leftrightarrow KCl_{gas}. \qquad (2)$$

From their equilibrium constants

$$\log a_{KCl_{melt}} = \log a_{KCl_{gas}} - \log K_2 = \log \frac{a_{HCl_{gas}}}{a_{H_2O_{gas}}^{1/2}} \qquad (3)$$
$$+ \log a_{K_2O_{melt}} + \log K_1.$$

Consequently, for a non-crystallizing melt (i.e. $X_{K2O} = $ const), an increase in the $a_{HCl_{gas}}/a_{H_2O_{gas}}^{1/2}$ ratio causes an increase of $a_{KCl_{melt}}$, and hence $X_{KCl_{melt}}$. Because at constant pressure this ratio would increase in response to CO_2-fluxing and dehydration, reaction (1) explains experimental data showing that the Cl fluid–melt partition coefficient decreases when CO_2 is added to an H_2O–Cl–melt system (Alletti *et al.*, 2009). Similar to the mechanism proposed to explain increasing Cl contents in zoned hornblende (Humphreys *et al.*, 2009), this suggests that Cl and K enrichment in a melt can be an indirect consequence of the transfer of a CO_2-dominated, KCl-bearing gas phase fluxing through the magmatic system at variable depths. To a lesser extent, this process could also induce Ca enrichment, because of the presence of $CaCl_2$ in the magmatic gases (Symonds & Reed, 1993) that infiltrate the plumbing system. However, the predominance of K enrichment makes gas fluxing a process that essentially occurs at constant CaO (Fig. 5c and d).

It is worth noting that fluid percolation through the magmatic plumbing system has already been invoked as one of the processes responsible for the anomalous enrichment in K, Sb, Cl and F at CF (Villemant, 1988), Procida (Mormone *et al.*, 2011) and Mt. Etna (Ferlito & Lanzafame, 2010, and references therein). In magmas erupted at SV, volatile influx has also been inferred to account for a $\delta^{18}O$ increase (with decreasing MgO) (Ayuso *et al.*, 1998), although the main agent for the potassium enrichment in the SV eruptive products (tending to ultra-potassic) must be sought in either phlogopite in the mantle source (Peccerillo, 2005, and references therein) or crustal contamination by limestone (Iacono-Marziano *et al.*, 2009).

Magma crystallization and degassing: the redox connection

An intriguing observation is the nearly constant, low MgO contents (∼3·6 wt %; Fig. 5a) in the Ischia K-trachybasaltic and shoshonitic MI trapped in olivines covering a broad compositional range (Fo from 79 to 89 mol %), as well as in the few analyzed clinopyroxenes. This feature is shared with some weakly evolved CF and SV products (Marianelli *et al.*, 1999; Mangiacapra *et al.*, 2008; unpublished data by the authors), whereas the primitive eruptive products of the neighbouring Procida volcanic field (Fig. 1), although geochemically almost

indistinguishable (e.g. Peccerillo, 2005), are characterized by MgO contents of up to ~12 wt %, as shown by both whole-rocks (D'Antonio *et al.*, 1999*a*) and MI hosted in highly forsteritic olivine (Fo = 85–90 mol %; Severs, 2007; Esposito *et al.*, 2011; Mormone *et al.*, 2011). If we discard the hypothesized post-entrapment evolution of MI, their low Mg content could be a primary feature resulting from fast growth of the MI-trapping olivine crystals, with consequent relative Mg-enrichment in the host crystal and Mg-depletion in the trapped melt. However, this process should lead to zoned olivines, which have not been observed in the analyzed samples (Table 1; Supplementary Data). Moreover, such a mechanism does not necessarily account for the observed MgO buffering around 3·6 wt % (Fig. 5a), and demands that Mg diffusion in the liquid is slower than the crystal growth. Because diffusion does not occur at a constant rate, it is useful to compare the time needed by diffusion to cover a characteristic diffusion distance with the time required by olivine to grow by the same length.

Following Zhang (2008), we define the diffusion distance as that for which the concentration of MgO in the melt is halfway between the hypothetical compositional extremes. Specifically, the diffusion distance is halfway between the primitive Procida melt composition and the analyzed Ischia MI. We then consider $x_{mid} = \gamma (Dt)^{1/2}$, where x_{mid} is the mid-concentration distance, D is the Mg-diffusion coefficient ($\sim 10^{-13}$ m^2 s^{-2} at the temperature of interest; Roselieb & Jambon, 2002), γ takes the value of 0·95 for half-space diffusion, and t is time. Assuming the size of MI as a diffusion distance ($x_{mid} = 100\,\mu m$), 110 000 s are needed to reach mid-concentration (i.e. Mg-diffusion is around 100 times faster than olivine growth) by considering a crystal growth rate around 10^{-11} m s^{-1} [i.e. comparable with, or even faster than, those of olivines in basalt (Mangan, 1990)]. Assuming a value of x_{mid} close to 1 cm [i.e. exceeding the size of the largest Ischia olivines (3–4 mm)], Mg-diffusion and crystal growth yield comparable timescales (~30 years), a condition that still ensures crystal–melt chemical equilibrium. Therefore, we discard the role of competing diffusive processes in the melt and crystal growth in determining the lower MgO content of Ischia MI with respect to those from Procida.

In line with a recent study of Hawaiian magmas (Matzen *et al.*, 2011), we link the low Mg content of the Ischia MI to a high redox state. The Ischia MI provide an excellent example in which divalent and trivalent iron species are abundant in the system and in equimolar proportions, thus appearing as the effective redox couple buffering the oxygen potential of the whole system and imposing the low-Mg conditions for the liquid–olivine equilibrium ($K_D = 0·3$; Roeder & Emslie, 1970). Tests run with the MELTS code (Ghiorso & Sack, 1995) show that an Ischia melt composition with MgO ~4 wt % can

precipitate a forsteritic olivine (Fo = 85 mol %) only at NNO >3, for a temperature of 1180°C, dissolved $H_2O = 3$ wt % and P set at 3 kbar (roughly in line with our MI results). Under these conditions, Fe^{2+}/Fe^{3+} is ~1. More forsteritic olivine (up to Fo_{90}) can be obtained, at (liquidus) temperatures of 1210°C, by further increasing the oxidation state up to NNO $\approx$ +5. For lower oxygen fugacity, such as NNO, the crystallizing olivine is more fayalitic (Fo = 78 mol %; $T = 1120$°C). By raising the MgO content of the initial melt to 8–9 wt %, highly forsteritic olivines (Fo ~90 mol %) are at the liquidus for more normal redox conditions (i.e. between QFM and NNO) and for relatively higher temperatures of either 1250°C, if dissolved $H_2O = 3$ wt %, or 1270°C, if dissolved $H_2O = 1$ wt %. The latter is the case for the most primitive Procida volcanic products, as indicated by (1) the occurrence of H_2O-poor MI in highly forsteritic olivines ($H_2O < 2$ wt %; 85 mol % < Fo < 90 mol %; Severs, 2007; Esposito *et al.*, 2011; Mormone *et al.*, 2011), (2) measured $FeO/Fe_2O_3 \sim 3$ (by weight) in whole-rocks (D'Antonio *et al.*, 1999*a*), and (3) estimated $FeO/Fe_2O_3 \sim 2$ (by weight) in MI (Mormone *et al.*, 2011), which requires Fe^{2+} being dominant over Fe^{3+} to attain the olivine–liquid equilibrium (or $K_D = 0·3$).

Although such high oxidation state conditions challenge the MELTS software limits, these results corroborate the interrelation between an unusually high oxidation state (ΔNNO > 3), high olivine forsterite contents (85–90 mol %) and low (~4 wt %) MgO contents of the analyzed Ischia MI. Moreover, the high oxidation states predicted here are consistent with recent evidence that sub-arc mantle is 1–4 log units more oxidized than mid-ocean ridge basalt (MORB)- or ocean island basalt (OIB)-source mantle (Evans *et al.*, 2012) and, particularly, with the fO_2 estimates from Ischia Cr-rich spinel inclusions. Application of the Maurel & Maurel (1982) equation to these samples predicts relative fO_2 values falling between NNO + 1·5 and NNO + 3·3 for mafic magmas equilibrated with Fo_{89} olivines (D'Antonio *et al.*, 2013). The lower fO_2 value is relative to MI compositions corrected for the effects of post-entrapment crystallization of olivine (re-equilibrated dataset), whereas the second value relates to the original dataset. Also, for the first and most conservative case (NNO + 1·5), Ischia shows the most oxidized source conditions so far recognized for central–southern Italian magmas (Nikogosian & Van Bergen, 2010; D'Antonio *et al.*, 2013).

It is important, however, to note the impossibility of coupling the Cr-spinel data with the whole-rock compositions of Ischia mafic magmas in the frame of the the Maurel & Maurel (1982) equation. Primitive Ischia whole-rocks have FeO_{tot}/MgO values lower than the $(Fe^{II}O/MgO)_{Maurel\&Maurel}$ melt ratio (0·9 from Cr-spinels hosted in Fo_{89} olivines). Therefore, the whole-rocks, probably

because of olivine accumulation, do not have enough iron to be representative of the parental magmas. On the other hand, the MI, with their low MgO and FeO_{tot}/$MgO > 1 > (Fe^{II}O/MgO)_{Maurel \& Maurel}$, can be considered as such.

The large difference in oxidation state between the Ischia and Procida magmas probably results from variations in the amount of water, which is much greater at Ischia (up to 4 wt %) than at Procida (<2 wt %; Severs, 2007; Esposito *et al.*, 2011; Mormone *et al.*, 2011). For temperatures below 1200°C along the geothermal gradient, and in the presence of abundant water, the magma continues evolving along the olivine liquidus by substantially increasing the oxidation state of the system.

Owing to the large proportion of oxygen they carry, H_2O–CO_2 fluids oxidize any magmas that they permeate. On the one hand, recently it has been shown that strong iron oxidation, caused by CO_2 fluxing, produces a maximum local oxygen fugacity around $NNO + 3$ to $NNO + 3.5$ (Simakin *et al.*, 2012). On the other hand, the possible role of H_2O as an oxidizing agent in magmas has been explored by Kelley & Cottrell (2009), who showed its efficiency in subduction environments for its enhanced mobility in the fluid phase transferred from the slab. Although the subducting plate is intrinsically at a high oxygen fugacity, and clearly supplies the H_2O flux into the overlying mantle wedge, the mechanism by which the oxidized signature is transferred from the slab is poorly understood. The above researchers have suggested that the relation between Fe oxidation state and magmatic H_2O content at subduction zones may result from the oxidized state of the subducted oceanic lithosphere (e.g. iron in marine sediments is highly oxidized; Fe^{2+}/Fe^{3+} ~0·22). It is likely that supercritical fluids released from the de-volatilizing slab form aqueous complexes of oxidized iron that migrate upwards, transferring their oxidized signature to the resultant mantle wedge melts (e.g. Gaetani & Grove, 2003). Nevertheless, adoption of this model for iron oxidation (Ottonello *et al.*, 2001; Moretti, 2005) shows that for a given fO_2, increasing the water fugacity, and hence the water content in the melt, decreases the Fe^{2+}/Fe^{3+} ratio, without the necessity of invoking any transfer of oxidized iron complexes from the de-volatilizing slab (Moretti & Ottonello, 2003; Moretti & Papale, 2004).

Additional evidence for the Ischia high oxidation state is provided by S degassing. In fact, a high oxidation state, well above NNO, favours S dissolution in the melt (Moretti & Papale, 2004), retarding its release to late depressurization stages. Based on the available MI data for the Ischia and Procida K-trachybasalts, we have modelled the S behaviour choosing an initial value S ~1500 ppm, corresponding to the S content of the deepest MI (hosted

in a Fo_{86} olivine; Fig. 9) among those analyzed for S (Table 1). Moreover, a value of 1500 ppm for S content was also measured in the least evolved, most CO_2-rich MI from Procida (Esposito *et al.*, 2011; Mormone *et al.*, 2011) and in the least degassed shoshonitic MI from CF (Mangiacapra *et al.*, 2008). Because of the very high S solubility at high pressure under oxidized conditions, we assumed its initial content to be representative of the total amount in the parental magma and used it to model the different conditions of sulphur release between Procida and Ischia.

Model runs for degassing in the CO_2–H_2O–H_2S–SO_2– melt system (Moretti & Papale, 2004) for a non-crystallizing magma ascending in closed system, clearly show that under oxidizing conditions (fixed by Fe^{2+}/$Fe^{3+} = 1$, corresponding to $NNO + 3$) the system does not degass appreciably, and keeps its initial value of S at 1500 ppm down to a dissolved H_2O content less than 1 wt % or 20 MPa (dashed black curves in Fig. 9a and b, respectively). Conversely, if the Fe^{2+}/Fe^{3+} ratio is around 10 (corresponding to $log fO_2$ around NNO) S degassing takes place immediately, resulting in a complete loss of S at H_2O content less than 1 wt % or in a loss of 400 ppm of S at 300 MPa (dotted black curve in Fig. 9a and b), in response to the lower solubility of S with respect to water under reduced conditions. For an oxygen fugacity corresponding to $NNO + 1.5$ (i.e. considering the re-equilibrated MI compositions) S-degassing takes place at around 280–300 MPa (continuous black line in Fig 9b).

These behaviours well discriminate reduced and oxidized domains in the S vs H_2O and S vs pressure diagrams (Fig. 9a and b), but cannot explain the S-enrichment up to 2300 ppm. Such an enrichment can, however, be accounted for by considering the joint effect of crystallization and fluid fluxing. The amount of fractional crystallization has been evaluated using the Petrograph 2beta code (Petrelli *et al.*, 2005), using the composition of two analysed MI, ICn2 ol5 and Vat A ol6, representative of a primitive and a more evolved Ischia melt, respectively (Table 1). The results suggest that the daughter magma can be derived from the parent magma by subtraction of *c.* 36 wt % of a mineral assemblage dominated by Mg-rich clinopyroxene and Ca-rich plagioclase, with a small amount of K-feldspar, Mg-rich olivine and Ti-magnetite ($\Sigma r^2 = 0.55$; see Supplementary Data for details).

The role of crystallization is then introduced into the modelling by using the following simple linear relationship, which returns 36 wt % of crystallization from 500 MPa to 0·1 MPa:

$$M_{xx}(\text{wt\%}) = -0.07P(\text{MPa}) + 34.9 \qquad (4)$$

in which M_{xx} is the amount of crystallized magma. The value of 500 MPa for the beginning of crystallization is
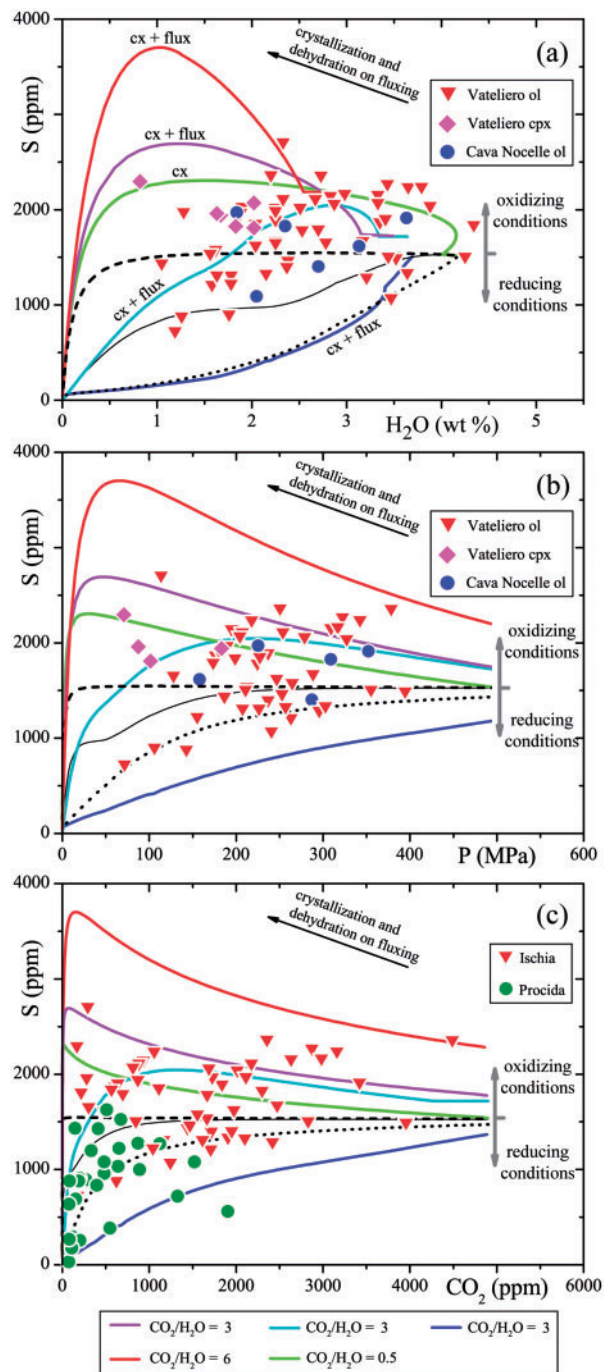
Fig. 9. Effects of crystallization, redox state, fluxing and depressurization on S concentration in multicomponent degassing melts. Dashed, continuous and dotted black curves in (a)–(c) represent closed-system degassing ($H_2O^{tot} = 4\cdot25$ wt %, $CO_2^{tot} = 2\cdot1$ wt %, $S^{tot} = 0\cdot15$ wt %) of the 'unfluxed' and non-crystallizing magma ($Fe^{3+}/\Sigma Fe = 0\cdot5$ for the dashed curve, $Fe^{3+}/\Sigma Fe = 0\cdot3$ for the continuous curve, calculated by using the composition of the MI corrected for post-entrapment crystallization). The dotted black curve refers to reduced conditions. Bold coloured lines in (a)–(c) account for crystallization, and for different degrees of CO_2 enrichment, given as a mass ratio with respect to H_2O. Green, magenta and red curves were calculated for $Fe^{3+}/\Sigma Fe = 0\cdot5$, varying CO_2^{tot}/H_2O^{tot} from 0·5 to

close to the largest computed saturation pressure (480 MPa for the re-equilibrated MI dataset). Crystallization alone, without fluxing, generates a degassing curve under closed-system conditions that preserves the initial CO_2^{tot}/H_2O^{tot} ratio (0·5 by mass), demands initial H_2O enrichment, and can only partially account for the high S values (higher than 2000 ppm) at low pressure and water contents (turquoise line in Fig. 9a and b). It is also necessary to introduce the effect of fluxing (by adding CO_2 and increasing the CO_2^{tot}/H_2O^{tot} ratio from 0·5 to three and then to six by mass) to achieve degassing patterns matching the high S points in both diagrams (magenta and red curves in Fig. 9a and b).

A major outcome of our modelling is that only the combination of (1) high oxidation state, (2) crystallization on magma ascent [in terms of simple mass removal based on equation (4)] and (3) fluxing and consequent melt dehydration allows reproduction of the high-S (>2000 ppm)–low-H_2O (<1 wt %) data points. If the system is reduced (Fig. 9a and b), S solubility is so depressed that fluid fluxing ($CO_2^{tot}/H_2O^{tot} = 3$ by mass) and crystallization (blue curves in Fig. 9a and b) do not reproduce the S enrichment, and melt desulphurization occurs, as for dehydration. The latter is very probably the case for S in the Procida MI (Severs, 2007; Esposito *et al.*, 2011; Mormone *et al.*, 2011), which is much less abundant than in the Ischia MI, at a similar CO_2 content (Fig. 9c). This suggests that S was stripped into the gas phase under much more reduced conditions (Moretti & Papale, 2004).

The alkali variability and the constancy of iron oxidation state, as well as the MgO content of the non-corrected MI compositions, lead us to conclude that the dehydration displayed by the MI is due to CO_2-fluxing rather than diffusive re-equilibration of water driven by proton diffusion (e.g. Massare *et al.*, 2002; Gaetani *et al.*, 2011). In fact, proton diffusion would alter the Fe^{2+}/Fe^{3+} ratio, thus producing scattered values. On the other hand, a full-equilibrium scenario allows modelling of all the data, including S loss.

Fig. 9 Continued

three up to six by mass; the cyan curve is for $Fe^{3+}/\Sigma Fe = 0\cdot3$ and $CO_2^{tot}/H_2O^{tot} = 3$ by mass (see Appendix). The dark blue line accounts for crystallization and fluxing ($CO_2^{tot}/H_2O^{tot} = 3$ by mass) under reduced conditions. (c) illustrates the CO_2 vs S covariation in MI from Ischia (this study) and Procida (Severs, 2007; Esposito *et al.*, 2011; Mormone *et al.*, 2011), starting from a common initial S content of 1500 ppm. Accounting for fluxing + crystallization yields S enrichment only under oxidized conditions (i.e. Ischia); that is, for $Fe^{3+}/\Sigma Fe \geq 0\cdot3$ (or log $fO_2 \geq NNO + 1\cdot5$). The higher the oxidation state, the greater the melt enrichment in S. In contrast, reduced conditions (i.e. Procida) do not favour S enrichment, leading to S depletion even at high dissolved CO_2 contents (i.e. pressure). The black arrow in the upper right of (a) is a qualitative vector indicating that coupled crystallization and fluxing of a melt evolving under oxidizing conditions yields strong dehydration and S enrichment).

Geodynamic relations and the role of ascending CO_2-dominated fluids in determining magma evolution at Ischia and the other Neapolitan volcanoes

The information provided thus far by the MI data makes the Ischia magmatic plumbing system a natural crustal borehole that can shed light on melt–fluid coexistence conditions, particularly on the presence of a CO_2-dominated supercritical fluid phase rising from mantle depths. Such knowledge, together with the available data for the other Neapolitan volcanoes, can be used to investigate the relationships between these volcanoes, which all have plumbing systems extending to mantle depths (Peccerillo, 2005).

The Neapolitan volcanoes show striking morphostructural similarities, highlighted by seismic reflection data (Bruno et al., 2003), magnetic data (Paoletti et al., 2009), and the relationships between the location of eruptive vents and magma compositions (Civetta et al., 1991; D'Antonio et al., 1999b; Piochi et al., 2005; De Astis et al., 2006; Di Renzo et al., 2011). Ischia and CF are located at the intersection of NE–SW- and NW–SE-trending fault systems, and are characterized by large, caldera-forming eruptions and resurgence of the caldera floor, suggesting the presence of large, shallow magma chambers. Both volcanoes mostly extruded differentiated (trachyte–phonolite) magmas during the caldera-forming eruptions through vents located within the caldera floor. Weakly differentiated magmas (shoshonite–latite) have been erupted only by vents located along portions of faults of the NE–SW system, most of which have acted as marginal faults during caldera collapses (e.g. the Arso, Vateliero and Cava Nocelle eruptions at Ischia, and the Minopoli and Fondo Riccio eruptions at CF). Conversely, the Procida volcanic field has erupted relatively small volumes of mainly weakly differentiated magma (K-basalt to shoshonite) through vents aligned along faults of the NW–SE transfer system. Trachytic to phonolitic Plinian and sub-Plinian eruptions, accompanied by summit caldera collapses at SV, are located at the intersection of the NE–SW and NW–SE fault systems, also suggesting the presence of a large, shallow magma chamber.

The geochemical relationships between the parental magmas can be considered in terms of their Sr and Nd isotopic compositions and the high field strength element (HFSE/HFSE) (Nb/Zr) ratio along an idealized transect from the Tyrrhenian Sea [MORB: Ocean Drilling Program (ODP) Leg 107, site 655 on the Gortani Ridge, western Vavilov Basin; Gasperini et al., 2002, and references therein], through Ischia, Procida, CF and SV (Fig. 10). The plotted isotopic and chemical data refer to CF rocks younger than 39 ka (i.e. before the caldera-forming Campanian Ignimbrite eruption; Fisher et al., 1993), and SV rocks older than 22 ka. These were selected because they do not show significant evidence of crustal
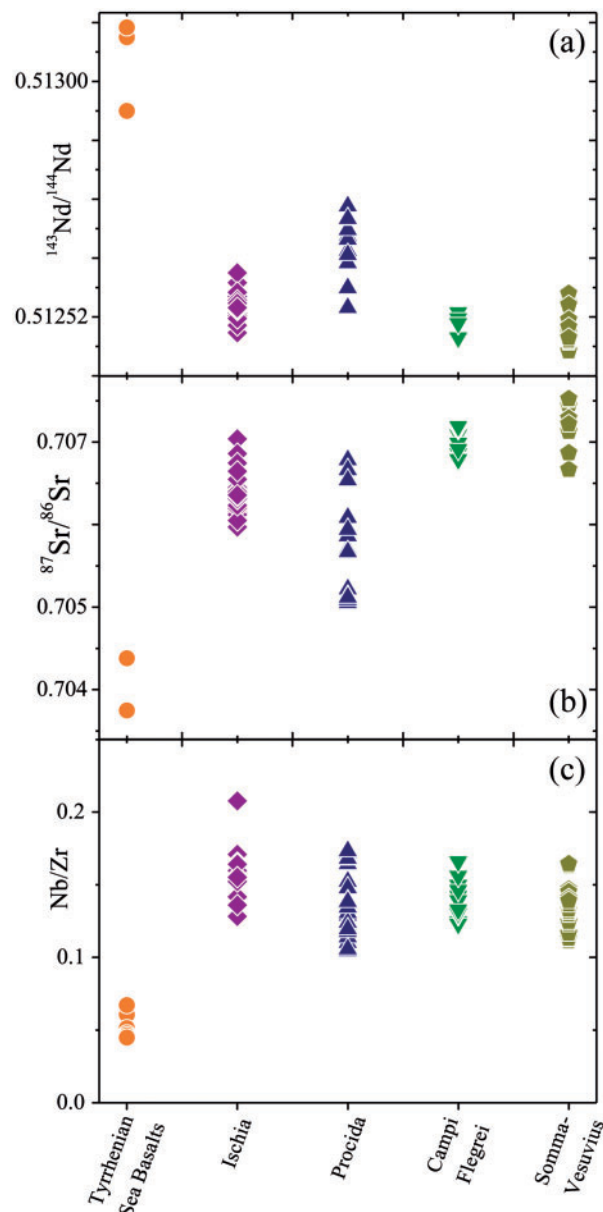
Fig. 10. Nd (a) and Sr (b) isotope, and Nb/Zr (c) variations along an idealized transect extending from the Tyrrhenian Sea through the Neapolitan volcanoes. Data from Gasperini et al. (2002), Pappalardo et al. (2002), De Astis et al. (2004, 2006), Piochi et al. (2004), D'Antonio et al. (2007), Di Renzo et al. (2007) and Pabst et al. (2008).

contamination, unlike the younger products (e. g. Pappalardo et al., 2002; D'Antonio et al., 2007; Di Renzo et al., 2007, 2011). The Ischia magmas are geochemically and isotopically similar to the SV least contaminated magmas older than 22 ka and the CF magmas younger than 39 ka (D'Antonio et al., 2007).

All the Neapolitan volcanoes have a similar geochemical signature (e.g. Nb/Zr ratio), which is different from that of the Tyrrhenian Sea basalts, despite differences in

composition and eruptive style, and variable amounts of crustal assimilation, mixing, and fractional crystallization during their evolution to recent times (e.g. Civetta *et al.*, 1991; Ayuso *et al.*, 1998; Fulignati *et al.*, 1998; Piochi *et al.*, 1999; Gilg *et al.*, 2001; Tonarini *et al.*, 2004; De Astis *et al.*, 2006; D'Antonio *et al.*, 2007; Di Renzo *et al.*, 2007, 2011; Arienzo *et al.*, 2009, 2011; Iacono-Marziano *et al.*, 2009, and references therein).

The geochemical signature of all the Neapolitan volcanoes (Fig. 10) reflects the involvement of either a MORB-type (D'Antonio *et al.*, 2007, and references therein) or an OIB-type mantle source (De Astis *et al.*, 2006, and references therein), partially modified by subducting slab derived fluids and melts.

Procida is located between CF and Ischia (Fig. 1) along a NE–SW strike-slip tectonic feature that approximately follows the dip of the subducting slab. With such a configuration, and contrary to what is observed, a larger involvement of the water-poor, MORB- (or OIB)-type mantle source component would be expected at Ischia rather than Procida, because the former is located at a greater distance from the subducting slab, which dips towards the Tyrrhenian Sea. A possible explanation for such an unexpected result could be in the crystallization of magmas ponding at mid-crustal depths: the larger the extent of crystallization, the higher the degree of water enrichment, as differentiation tends to concentrate the most soluble volatile components. However, this explanation is not supported by the very limited chemical difference between Ischia and Procida MI (Fig. 2a and b). An alternative hypothesis is that the difference in initial H_2O concentration ($\sim$4 wt % at Ischia and <2 wt % at Procida), reaching the highest values at greatest depth ($\sim$14 km at Procida and $\sim$18 km at Ischia), indicates a different H_2O content in the deep slab-derived fluid source. The lower H_2O/CO_2 ratio in the source below Procida could be related to a larger contribution of a (water-poor) transitional (T)-MORB (or OIB) mantle source component than at Ischia, CF and SV, as supported by the variation of large ion lithophile elements (LILE) relative to HFSE (not shown), and radiogenic isotopes in the products of these volcanic systems (Fig. 10). However, owing to the location of Ischia and CF with respect to Procida, such a hypothesis would need a nearly punctiform slab breakthrough or tear to allow the ascent of the 'pristine' mantle component below Procida. Similarly, changes in H_2O content related to slab surface temperature (Plank *et al.*, 2009) would demand a very localized peak of temperature, which again would be in contradiction to the relative location of CF, Procida and Ischia with respect to the subducting slab. At subduction zone depths (>100 km; e.g. Chiarabba *et al.*, 2008) these two scenarios seem very unlikely in light of the short Ischia–Procida and Procida–CF distances (<5 km). Moreover, published data (Fig. 10)

reveal that the higher content of magmatic H_2O at Ischia, CF and SV (up to 4 wt %) with respect to Procida (<2 wt %) (Severs, 2007; Mormone *et al.*, 2011), and the consequent difference in redox state, is reflected in the geochemical signature of the eruptive products. They show an appreciable difference between Procida on the one side and Ischia, CF and SV on the other side. In fact, whereas the HFSE/HFSE ratios (Nb/Zr) are similar for all these volcanoes, pointing to a common pre-subduction mantle, different Sr, Nd, Pb and B isotope ratios (the latter two not shown) for Procida with respect to the other volcanoes require a different mobilization of deep slab-derived fluids in the overriding plate.

We suggest that the heterogeneity of the highly oxidized Campanian mantle source region is due to large volumes of hot, CO_2-rich, oxidizing fluids coming from subduction slab-derived pelagic sediments (D'Antonio *et al.*, 2013), which can explain the observed variability in the chromium number of olivine-hosted spinels in the Neapolitan volcanic rocks.

The above geochemical features, and the initial water contents, which are lower at Procida than at the other Neapolitan volcanoes, could be related to the areal distribution and interplay between the NW–SE normal faults and the NE–SW transfer faults dissecting the Campanian Plain. Following Doglioni (1996) and Italiano *et al.* (2000), we postulate that the faults affecting the Neapolitan volcanic area are deep lithospheric structures. They permit the ascent of fluids released from the subducted slab that accumulate at the base of the lithosphere. These are mostly tapped beneath Ischia, CF and SV, where the intersecting fault systems generate a particularly high crustal permeability, thus favouring not only ascent of deep fluids or melts but also their horizontal drainage and the formation of large magma chambers (Figs 1 and 11). Crustal dissection also favours accumulation of deep fluids involved in caldera resurgence processes.

The characteristics of the Procida magma feeding system, such as (1) the relatively small amount of H_2O in the parental melts, (2) isotopic compositions less enriched in radiogenic Sr, Pb and unradiogenic Nd, and (3) modest amounts of magma production, are inferred to be a consequence of the reduced input of deep fluids, owing to the lower crustal permeability compared with that beneath Ischia, CF and SV. Fluid connectivity at Procida is achieved only occasionally, thus preventing long-term crustal storage of magma and fluids, which are directly transferred to the surface along the transfer fault planes, whenever they are characterized by strong vertical permeability. From this perspective, the pressure interval for relatively fast magma ascent at Procida (from 350 MPa to volcanic venting; Mormone *et al.*, 2011) can be taken as a rough measure of the depth reached by the transfer faults (13–14 km). The relatively short residence

time of fluids and melts below Procida (compared with Ischia, CF and SV) owing to such a straight connection from mid-crustal depths to the surface is also supported by the high $^3He/^4He$ values at Procida (around 5 R/Ra; Piochi *et al.*, 2005). In contrast, $^3He/^4He$ values are significantly lower wherever large magma bodies have formed in the crust at the intersection of NE–SW and NW–SE tectonic features, and where there is more pronounced addition of radiogenic He from the crust (Chiodini *et al.*, 2010).

The structural conditions generated by the intersection of the NW–SE normal faults and NE–SW transfer faults below Ischia, CF and SV are suitable for the formation of large magma chambers and large residual crystal mushes (e.g. De Natale *et al.*, 2006; D'Antonio, 2011; see below) in which interaction with deep fluid and new magma batches can explain why the Ischia and CF products record strong mineralogical and isotopic disequilibria (Civetta *et al.*, 1991; Di Renzo *et al.*, 2011).

Another interesting similarity between Ischia, CF and SV is the common occurrence of one or more mid-crustal low-velocity layers, at least 1 km thick (e.g. Auger *et al.*, 2001), lying roughly at the same depth below the volcanoes. The extent of such layers at 8–9 km depth (equivalent to a pressure of ~200 MPa) suggests some lateral continuity between the magma storage systems within the Neapolitan volcanic area. This layer is volatile-rich and acts as a valve controlling the upward transfer of magmas and fluids, giving rise to shallower magma chambers that feed both hydrothermal systems and surface eruptions. We speculate that the occurrence of such a mid-crustal magma reservoir may be linked to the widespread CO_2-dominated plume rising through the crust (e.g. Chiodini *et al.*, 2004; Frezzotti *et al.*, 2009) and infiltrating the volcanic plumbing systems through the deep lithospheric faults that dissect both crust and mantle on a small scale (Acocella & Funiciello, 1999). The occurrence of such lithospheric faults also within the Apennine chain (Italiano *et al.*, 2000; Chiodini *et al.*, 2004, 2010) may suggest efficient drainage of the same deep slab-derived fluids through the crust, enhanced by the presence of CO_2 (Fig. 11). Not surprisingly, and despite the absence of detectable deep magma bodies, He isotope ratios in the Southern Apennines reach maximum values (5–6 R/Ra) in those areas characterized by the largest CO_2 emissions (at Mefite d'Ansanto; Chiodini *et al.*, 2010; see also Fig. 11).

The generation of supercritical fluids owing to deep CO_2 release is thus an important process within the Neapolitan volcanic region, as evidenced by: (1) widespread and deep-generated diffuse CO_2 degassing (both at volcanic and non–volcanic sites; Chiodini *et al.*, 2004, 2010; Frezzotti *et al.*, 2009); (2) the occurrence of CO_2-rich melts at all the Neapolitan volcanoes (Marianelli *et al.*, 1999, 2005; Severs, 2007; Mangiacapra

et al., 2008; Arienzo *et al.*, 2010); (3) evidence for fluid transfer (fluxing) through the magmatic systems at CF (Villemant, 1988; Mangiacapra *et al.*, 2008; Arienzo *et al.*, 2010), Procida (Mormone *et al.*, 2011) and SV (Ayuso *et al.*, 1998; Quareni *et al.*, 2007); (4) low P-wave seismic velocity, high seismic attenuation, and high anomalies in P/S wave velocity ratios. These data indicate that magmatic fluids are produced at a depth of about 150 km and stored in the lower crust or uppermost mantle (Chiarabba *et al.*, 2008).

The occurrence of an extensive plume of CO_2-dominated fluid, rising from great depth along preferential lithospheric pathways, highlights the important role of fluids in promoting chemical exchange (metasomatism) with the surrounding rocks (including the mantle wedge) and percolated magmas (e.g. Berkesi *et al.*, 2012). Recently, the deep origin of such a gas plume was explained in terms of deep CO_2-rich magmas generated by melting of carbonated crustal rocks subducted at ~150 km depth, which release CO_2 because of depressurization on their ascent (Frezzotti *et al.*, 2009). Although we cannot precisely assess the exact origin of the widespread CO_2 emissions at the surface (e.g. breakdown vs melting of carbonated slab metasediments), we can confidently state that there is strong evidence that breakdown of limestones of marine origin at crustal depths plays only a minor role.

Within the Neapolitan area, Ischia samples the relatively most undisturbed supercritical fluid because interaction with the melt phase occurs under high fluid/melt ratios, as evidenced by both the total volatile content of the magmas (Fig. 7) and the huge discharge of magmatic fluids (Di Napoli *et al.*, 2009, 2011). Additionally, high fluid/melt ratios suggest that at great depths the ascending supercritical fluids may induce melting of existing crystal mushes (e.g. Gaetani & Grove, 2003) and then mobilize small batches of fluid-rich magma, contributing to Sr isotope disequilibrium between early olivine, diopside and glass (e.g. Piochi *et al.*, 1999).

In this context, the mafic magmas erupted at Ischia during the last 10 kyr could represent magma batches formed under hydrous and oxidized conditions by melting of a mush compositionally akin to the Procida mafic rocks. Iron is the most abundant multiple valence element within the magma mush system, and during fluid-induced melting it would buffer the redox state at $Fe^{2+}/Fe^{3+} \sim 1$ for the whole range of olivine compositions (from Fo_{79} to Fo_{89}) and non-corrected melt inclusion compositions (e.g. Giggenbach, 1996). This allows extraction from the mush of only the little Mg-content needed to achieve equilibrium with highly forsteritic olivine and would explain the occurrence of Mg-depleted and Mg-rich (MgO up to 12 wt %; Severs, 2007) MI within early crystallizing olivines ($Fo > 80$ mol %) from closely spaced, or even the same, magmatic reservoirs, such as those feeding the Ischia and
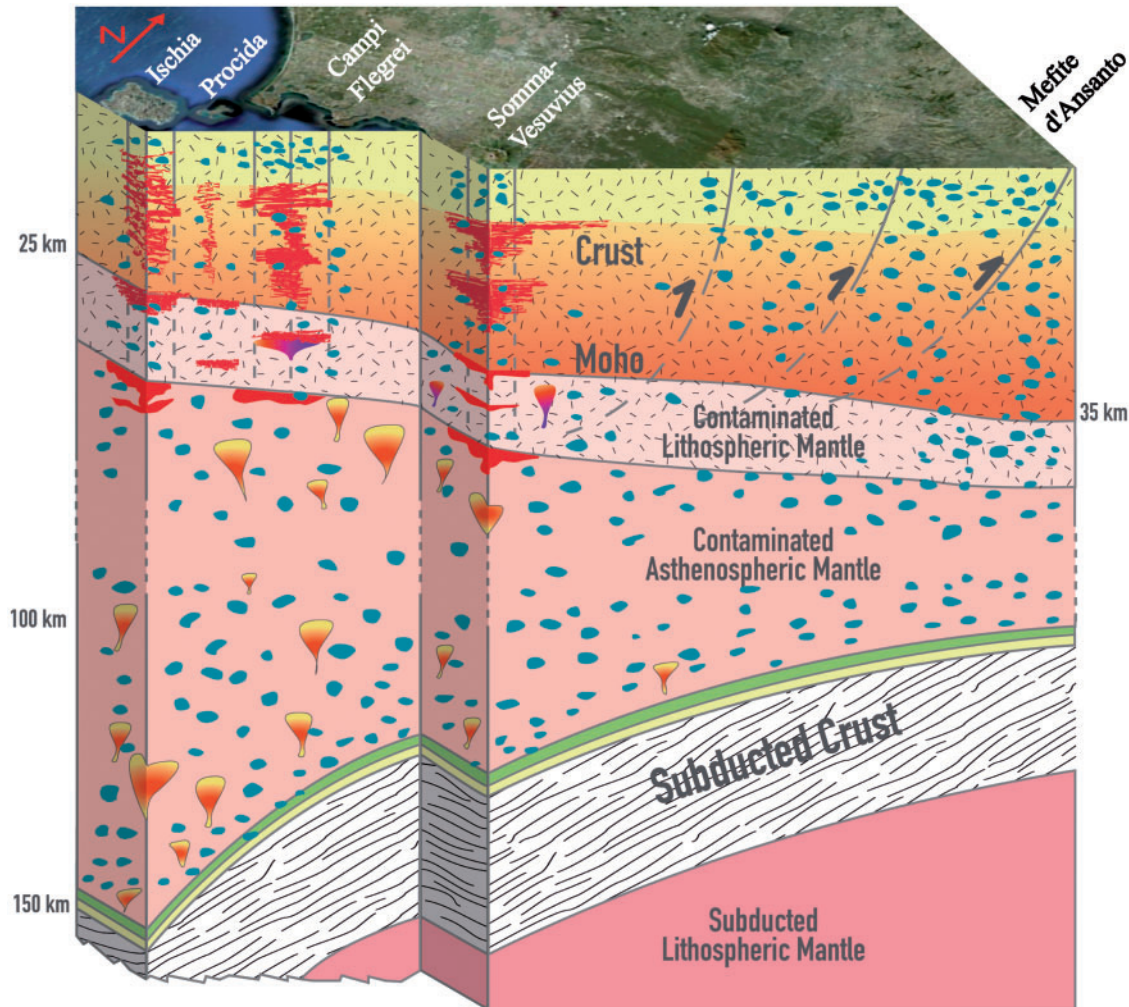
Fig. 11. Schematic cross-section of the asthenosphere and lithosphere below the Neapolitan volcanoes showing the relationships between the magmatic plumbing systems, the regional tectonic regime and the deep subduction system. A widely and uniformly degassing layer at the top of the subducting slab (down to ∼150 km depth beneath the Neapolitan volcanoes; Chiarabba *et al.*, 2008), related to the breakdown of CO_2–H_2O-bearing terrigenous and/or pelagic metasediments, supplies volatiles to the overlying asthenosphere and lithosphere, which are both contaminated by the ascent of supercritical fluids and melts. The asthenosphere is uniformly affected by exchange with the rising fluids. In contrast, the nearly 50 km thick lithosphere is contaminated by rising fluids along preferential paths coincident with the NE–SW transfer and NW–SE normal fault systems. In the Neapolitan region most of the magma transfer and accumulation occurs at the intersections between these two fault systems (Ischia, Phlegraean Fields and Somma–Vesuvius), whereas volcanic centres such as Procida that developed on top of the transfer fault system experience much less magma production. Traces of the NW–SE normal fault systems correspond to vertical shaded planes, whereas the NE–SW transfer fault systems are in the plane of the paper. Deep CO_2-rich fluids (but not magmas) also rise to the surface in the compressional setting of the Apennine chain (Fig. 1) along one such plane. (See text for further details.)

Procida volcanism. Moreover, mush remelting could generate Ca-rich MI but not the low CaO/Al_2O_3 (∼0·6) MI trapped in Fo > 87 olivines (e.g. I Cn2.7; Table 1), which alternatively could be explained by infiltration of residual melts not in equilibrium with their hosts.

A similar situation can be expected at CF and SV, where voluminous crystal mushes at depth have been suggested (De Natale *et al.*, 2006; D'Antonio, 2011), and mineralogical and isotopic disequilibria in the erupted magmas have been demonstrated (e.g. Di Renzo *et al.*, 2011, and references therein). Therefore, melting of crystal mushes by reactive porous fluid fluxing (e.g. Gaetani & Grove, 2003), and consequent magma chamber reactivation, is here suggested as much more likely than pure mantle diapirism.

CONCLUSIONS

This study has shown that an exsolved CO_2-rich gas phase coexists with Ischia magmas throughout the crust, at least in the upper 18 km. The emerging picture highlights a composite system with magma stored at variable depths that can experience both nearly isobaric degassing upon

crystallization (decrease of the CO_2/H_2O ratio) and crystallization upon dehydration (increase of the CO_2/H_2O ratio) owing to fluxing from deep crustal or even mantle depths. The occurrence of a fluxing phase, already identified at CF (Mangiacapra *et al.*, 2008; Arienzo *et al.*, 2010), explains the relatively low magma production compared with magmatic fluid discharge, especially if considering the potential role that fluid infiltration may play in remelting resident crystal mushes.

The mid-crustal 200–250 MPa fluid saturation zone (8–10 km depth) in the Ischia vertically extended magmatic plumbing system (3–18 km depth) provides evidence for a major region of magma stagnation and gas fluxing similar to CF (Mangiacapra *et al.*, 2008; Zollo *et al.*, 2008) and SV (Auger *et al.*, 2001). The occurrence of such a mid-crustal magma layer below the active Neapolitan volcanoes is rather surprising, but suggests a causal link common to the entire Neapolitan volcanic region. Such a causal mechanism involves the interplay between regional structures (NW–SE normal and NE–SW transfer faults) and a widespread deep volatile source, derived from subducting metasediments. The hypothesis that the Neapolitan magmatism and volcanism are sustained by CO_2-dominated supercritical fluids is corroborated by several lines of evidence, such as the widespread diffuse CO_2-rich gas emissions detected at the surface, seismic features compatible with deep (150 km) slab devolatilization and fluid accumulation in the mantle wedge, the occurrence of CO_2-rich melts, fluid fluxing through the magmatic systems, and metasomatic fluid release from subduction zone depths.

The efficiency of this deep fluid transfer from the subducting slab upwards varies according to the permeability of the overlying lithosphere. Permeability increases in those sectors in which NW–SE normal and NE–SW transfer fault systems intersect (Ischia, CF, and SV). Consequently, the different connectivity that can be established from subduction zone depths upwards also explains the variability in both H_2O content measured in the deep magmas (up to 4 wt % at SV, CF and Ischia and <2 wt % at Procida) and magma production rates. Intersection of NW–SE and NE–SW structures and consequent dissection of the lithosphere promotes variable ascent of subduction fluids contaminating the mantle wedge, hence offering a key to explain the geochemical similarities and differences between Procida, Ischia, CF and SV, and, particularly, the major variations in redox state that profoundly affect the chemistry (e.g. Mg content) of the magmas beneath the Neapolitan volcanic area.

The demonstration of a common volatile source component for the Neapolitan volcanism contributes to our understanding of the basic process of magma production at mantle depths and the transfer of these magmas to shallow levels where they differentiate, mix and mingle in magma chambers necessarily supersaturated in volatiles. Shedding light on the mechanisms that transfer magma and fluids from deeper to shallower levels of the magmatic plumbing systems improves our ability to understand the causes and dynamics of episodes of unrest taking place in one of the most densely populated volcanic areas of the world.

SUPPLEMENTARY DATA

Supplementary data for this paper are available at *Journal of Petrology* online.

REFERENCES

Acocella, V. & Funiciello, R. (1999). The interaction between regional and local tectonics during resurgent doming: the case of the island of Ischia, Italy. *Journal of Volcanology and Geothermal Research* **88**, 109–123.

Acocella, V. & Funiciello, R. (2006). Transverse systems along the extensional Tyrrhenian margin of central Italy and their influence on volcanism. *Tectonics* **25**, TC2003, doi:10.1029/2005TC001845.

Acocella, V., Funiciello, R., Marotta, E., Orsi, G. & de Vita, S. (2004). The role of extensional structures on experimental calderas and resurgence. *Journal of Volcanology and Geothermal Research* **129**, 199–217.

Aiuppa, A., Bertagnini, A., Metrich, N., Moretti, R., Di Muro, A., Liuzzo, M. & Tamburello, G. (2010). A model of degassing for Stromboli volcano. *Earth and Planetary Science Letters* **295**, 195–204.

Alletti, M., Baker, D. R., Scaillet, B., Aiuppa, A., Moretti, R., Shi, L. & Ottolini, L. (2009). Chlorine partitioning between a basaltic melt and H_2O–CO_2 fluids. *Chemical Geology* **263**, 37–50.

Anderson, A. T., Jr, Newman, S., Williams, S. N., Druitt, T. H., Skirius, C. & Stolper, E. (1989). H_2O, CO_2, Cl and gas in Plinian and ash flow Bishop rhyolite. *Geology* **17**, 221–225.

Arienzo, I., Civetta, L., Heumann, A., Wörner, G. & Orsi, G. (2009). Isotopic evidence for open system processes within the Campanian Ignimbrite magma chamber. *Bulletin of Volcanology* **71**, 285–300.

Arienzo, I., Moretti, R., Civetta, L., Orsi, G. & Papale, P. (2010). The feeding system of Agnano–Monte Spina eruption, Campi Flegrei (Italy): Dragging the past into present activity and future scenarios. *Chemical Geology* **270**, 135–147.

Arienzo, I., Heumann, A., Wörner, G., Civetta, L. & Orsi, G. (2011). Processes and timescales of magma evolution prior to the Campanian Ignimbrite eruption (Campi Flegrei, Italy). *Earth and Planetary Science Letters* **306**, 217–228.

Auger, E., Gasparini, P., Virieux, J. & Zollo, A. (2001). Seismic evidence of an extended magmatic sill under Mt. Vesuvius. *Science* **294**, 1510–1512.

Ayuso, R. A., De Vivo, B., Rolandi, G., Seal, I. R. & Paone, A. (1998). Geochemical and isotopic (Nd–Pb–Sr–O) variations bearing on the genesis of volcanic rocks from Vesuvius, Italy. *Journal of Volcanology and Geothermal Research* **82**, 53–78.

Barsanti, M., Papale, P., Barbato, D., Moretti, R., Boschi, E., Hauri, E. & Longo, A. (2009). Heterogeneous large total CO_2 abundance in the shallow magmatic system of Kilauea volcano, Hawaii. *Journal of Geophysical Research* **114**, B12201, doi:10.1029/2008JB006187.

Behrens, H., Misiti, V., Freda, C., Vetere, F., Botcharnikov, R. & Scarlato, P. (2009). Solubility of H_2O and CO_2 in ultrapotassic melts at 1200 and 1250°C and pressure from 50 to 500 MPa. *American Mineralogist* **94**, 105–120.

Belkin, H. E., De Vivo, B., Török, K. & Webster, J. D. (1998). Pre-eruptive volatile content, melt-inclusion chemistry, and microthermometry of interplinian Vesuvius lavas (pre-A.D. 1631). *Journal of Volcanology and Geothermal Research* **82**, 79–95.

Berkesi, M., Guzmics, T., Szabò, C., Dubessy, J., Bodnar, R. J., Hidas, K. & Ratter, K. (2012). The role of CO_2-rich fluids in trace element transport and metasomatism in the lithospheric mantle beneath the Central Pannonian Basin, Hungary, based on fluid inclusions in mantle xenoliths. *Earth and Planetary Science Letters* **331–332**, 8–20.

Blundy, J. & Cashman, K. (2008). Petrologic reconstruction of magmatic systems variables and processes. In: Putirka, K. D. & Tepley, F. J., III (eds) *Minerals, Inclusions and Volcanic Processes. Mineralogical Society of America and Geochemical Society, Reviews in Mineralogy and Geochemistry* **69**, 179–239.

Brown, R., Orsi, G. & de Vita, S. (2008). New insights into Late Pleistocene explosive volcanic activity and caldera formation on Ischia (southern Italy). *Bulletin of Volcanology* **70(5)**, 583–603, doi:10.1007/s00445-007-0155-0.

Bruno, P. P. G., Rapolla, A. & Di Fiore, V. (2003). Structural setting of the Bay of Naples (Italy) seismic reflection data: implications for Campanian volcanism. *Tectonophysics* **372**, 193–213.

Buchner, G., Italiano, A. & Vita-Finzi, C. (1996). Recent uplift of Ischia, southern Italy. In: McGuire, W. J., Jones, A. P. & Neuberg, J. (eds) *Volcano Instability on the Earth and other Planets. Geological Society, London, Special Publications* **110**, 249–252.

Cannatelli, C., Lima, A., Bodnar, R. J., De Vivo, B., Webster, J. D. & Fedele, L. (2007). Geochemistry of melt inclusions from the Fondo Riccio and Minopoli 1 eruptions at Campi Flegrei (Italy). *Chemical Geology* **237**, 418–432.

Chiarabba, C., De Gori, P. & Speranza, F. (2008). The southern Tyrrhenian subduction zone: Deep geometry, magmatism and Plio-Pleistocene evolution. *Earth and Planetary Science Letters* **268**, 408–423.

Chiodini, G., Cardellini, C., Amato, A., Boschi, E., Caliro, S., Frondini, F. & Ventura, G. (2004). Carbon dioxide Earth degassing and seismogenesis in central and southern Italy. *Geophysical Research Letters* **31**, L07615.

Chiodini, G., Caliro, S., Caramanna, G., Granieri, D., Minopoli, C., Moretti, R., Perrotta, L. & Ventura, G. (2006). Geochemistry of the submarine gaseous emissions of Panarea (Aeolian Islands, Southern Italy): magmatic vs. hydrothermal origin and implications for volcanic surveillance. *Pure and Applied Geophysics* **163**, 759–780.

Chiodini, G., Granieri, D., Avino, R., Caliro, S., Costa, A., Minopoli, C. & Vilardo, G. (2010). Non-volcanic CO_2 Earth degassing: Case of Mefite d'Ansanto (southern Apennines), Italy. *Geophysical Research Letters* **37**, L11303.

Cioni, R. (2000). Volatile content and degassing processes in the AD 79 magma chamber at Vesuvius. *Contributions to Mineralogy and Petrology* **140**, 40–54.

Cioni, R., Civetta, L., Marianelli, P., Métrich, N., Santacroce, R. & Sbrana, A. (1995). Compositional layering and syn-eruptive mixing of a periodically refilled shallow magma chamber: the AD 79 Plinian eruption of Vesuvius. *Journal of Petrology* **36(3)**, 739–776.

Cioni, R., Marianelli, P. & Santacroce, R. (1998). Thermal and compositional evolution of the shallow magma chambers of Vesuvius: Evidence from pyroxene phenocrysts and melt inclusions. *Journal of Geophysical Research—Solid Earth* **103(B8)**, 18277–18294.

Civetta, L., Gallo, G. & Orsi, G. (1991). Sr- and Nd-isotope and trace-element constraints on the chemical evolution of the magmatic system of Ischia (Italy) in the last 55 ka. *Journal of Volcanology and Geothermal Research* **46**, 213–230.

Collins, S. J., Pyle, D. M. & Maclennan, J. (2009). Melt inclusions track pre-eruption storage and dehydration of magmas at Etna. *Geology* **37**, 571–574.

Crisci, G. M., De Francesco, A. M., Mazzuoli, R., Poli, G. & Stanzione, D. (1989). Geochemistry of recent volcanics of Ischia Island, Italy: Evidences of crystallization and magma mixing. *Chemical Geology* **78**, 15–33.

D'Antonio, M. (2011). Lithology of the basement underlying the Campi Flegrei caldera: volcanological and petrological constraints. *Journal of Volcanology and Geothermal Research* **200**, 91–98.

D'Antonio, M., Civetta, L. & Di Girolamo, P. (1999a). Mantle source heterogeneity in the Campanian Region (South Italy) as inferred from geochemical and isotopic features of mafic volcanic rocks with shoshonitic affinity. *Mineralogy and Petrology* **67**, 163–192.

D'Antonio, M., Civetta, L., Orsi, G., Pappalardo, L., Piochi, M., Carandente, A., de Vita, S., Di Vito, M. A. & Isaia, R. (1999b). The present state of the magmatic system of the Campi Flegrei caldera based on a reconstruction of its behavior in the past 12 ka. *Journal of Volcanology and Geothermal Research* **91**, 247–268.

D'Antonio, M., Tonarini, S., Arienzo, I., Civetta, L. & Di Renzo, V. (2007). Components and processes in the magma genesis of the Phlegrean Volcanic District, southern Italy. In: Beccaluva, L., Bianchini, G. & Wilson, M. (eds) *Cenozoic Volcanism in the Mediterranean Area. Geological Society of America, Special Papers* **418**, 203–220, doi:10.1130/2007.2418(10).

D'Antonio, M., Tonarini, S., Arienzo, I., Civetta, L., Dallai, L., Moretti, R., Orsi, G., Andria, M. & Trecalli, A. (2013). Mantle and crustal processes in the magmatism of the Campania region: inferences from mineralogy, geochemistry, and Sr–Nd–O isotopes of young hybrid volcanics of the Ischia island (South Italy). *Contributions to Mineralogy and Petrology*, in press, doi:10.1007/s00410-013-0853.

Danyushevsky, L. V. & Plechov, P. (2011). Petrolog3: Integrated software for modeling crystallization processes. *Geochemistry, Geophysics, Geosystems* **12**, Q07021, doi:10.1029/2011GC003516.

Danyushevsky, L. V., Perfit, M. R., Eggins, S. M. & Falloon, T. J. (2003). Crustal origin for coupled 'ultra-depleted' and 'plagioclase' signatures in MORB olivine-hosted melt inclusions: evidence from the Siqueiros Transform Fault, East Pacific Rise. *Contributions to Mineralogy and Petrology* **144**, 619–637.

De Astis, G., Pappalardo, L. & Piochi, M. (2004). Procida volcanic history: new insights into the evolution of the Phlegraean Volcanic District (Campania region, Italy). *Bulletin of Volcanology* **56**, 622–641.

De Astis, G., Kempton, P. D., Peccerillo, A. & Wu, T. W. (2006). Trace element and isotopic variations from Mt. Vulture to Campanian volcanoes: constraints for slab detachment and mantle inflow beneath southern Italy. *Bulletin of Volcanology* **151**, 331–351.

Della Vedova, B., Bellani, S., Pellis, G. & Squarci, P. (2001). Deep temperatures and surface heat flow distribution. In: Vai, G. B. & Martini, I. P. (eds) *Anatomy of an Orogen: the Apennines and Adjacent Mediterranean Basins*. Dordrecht: Kluwer Academic, pp. 65–76.

De Natale, G., Troise, C., Pingue, F., Mastrolorenzo, G., Pappalardo, L., Battaglia, M. & Boschi, E. (2006). The Campi Flegrei caldera: unrest mechanisms and hazards. In: Troise, C., De Natale, G. & Kilburn, C. R. J. (eds) *Mechanisms of Activity and Unrest at Large Calderas. Geological Society, London, Special Publications* **269**, 25–45.

de Vita, S., Sansivero, F., Orsi, G., Marotta, E. & Piochi, M. (2010). Volcanological and structural evolution of the Ischia resurgent caldera (Italy) over the past 10 k.y. In: Groppelli, G. & Viereck-Goette, L. (eds) *Stratigraphy and Geology of Volcanic Areas. Geological Society of America, Special Papers* **464**, 193–241.

Di Girolamo, P., Melluso, L., Morra, V. & Secchi, F. A. G. (1995). Evidence of interaction between mafic and differentiated magmas in the youngest phase of activity at Ischia island (Italy). *Periodico di Mineralogia* **64**, 393–411.

Di Napoli, R., Aiuppa, A., Bellomo, S., Brusca, L., D'Alessandro, W., Gagliano Candela, E., Longo, M., Pecoraino, G. & Valenza, M. (2009). A model for Ischia hydrothermal system: Evidences from the chemistry of thermal groundwaters. *Journal of Volcanology and Geothermal Research* **186**, 133–159.

Di Napoli, R., Martorana, R., Orsi, G., Aiuppa, A., Camarda, M., De Gregorio, S., Gagliano Candela, E., Luzio, D., Messina, N., Pecoraino, G., Bitetto, M., de Vita, S. & Valenza, M. (2011). The structure of a hydrothermal system from an integrated geochemical, geophysical, and geological approach: The Ischia Island case study. *Geochemistry, Geophysics, Geosystems* **12**, Q07017, doi:10.1029/2010GC003476.

Di Renzo, V., Di Vito, M. A., Arienzo, I., Carandente, A., Civetta, L., D'Antonio, M., Giordano, F., Orsi, G. & Tonarini, S. (2007). Magmatic history of Somma–Vesuvius on the basis of new geochemical data from a deep bore-hole (Camaldoli della Torre). *Journal of Petrology* **48(4)**, 753–784, doi:10.1093/petrology/egl081.

Di Renzo, V., Arienzo, I., Civetta, L., D'Antonio, M., Tonarini, S., Di Vito, M. A. & Orsi, G. (2011). The magmatic feeding system of the Campi Flegrei caldera: Architecture and temporal evolution. *Chemical Geology* **281**, 227–241.

Di Vito, M. A., Arienzo, I., Braia, G., Civetta, L., D'Antonio, M., Di Renzo, V. & Orsi, G. (2011). The Averno 2 fissure eruption: a recent small-size explosive event at the Campi Flegrei Caldera (Italy). *Bulletin of Volcanology* **73**, 295–320, doi:10.1007/s00445-010-0417-0.

Dixon, J. A. & Pan, V. (1995). Determination of the molar absorptivity of dissolved carbonate in basanitic glass. *American Mineralogist* **80**, 1339–1342.

Doglioni, C., Harabaglia, P., Martinelli, G., Monelli, F. & Tito, G. (1996). A geodynamic model of the Southern Apennines accretionary prism. *Terra Nova* **8**, 540–547.

Edmonds, M., Aiuppa, A., Humphreys, M., Moretti, R., Giudice, G., Martin, R., Herd, R. A. & Christopher, T. (2010). Excess volatiles supplied by mingling of mafic magma at an andesitic arc volcano. *Geophysics, Geochemistry, Geosystems* **11**, Q04005.

Esposito, R., Bodnar, R. J., Danyushevsky, L. V., De Vivo, B., Fedele, L., Hunter, J., Lima, A. & Shimizu, N. (2011). Volatile evolution of magma associated with the Solchiaro eruption in the Phlegrean Volcanic District (Italy). *Journal of Petrology* **52**, 2431–2460.

Evans, K. A., Elburg, M. A. & Kamenetsky, V. S. (2012). Oxidation state of subarc mantle. *Geology* **19**, 783–786.

Ferlito, C. & Lanzafame, G. (2010). The role of supercritical fluids in the potassium enrichment of magmas at Mount Etna volcano (Italy). *Lithos* **119**, 642–650.

Fisher, R. V., Orsi, G., Ort, M. & Heiken, G. (1993). Mobility of a large volume pyroclastic flow emplacement of the Campanian Ignimbrite, Italy. *Journal of Volcanology and Geothermal Research* **56**, 205–220.

Frezzotti, M. L., Peccerillo, A. & Panza, G. (2009). Carbonate metasomatism and CO_2 lithosphere–asthenosphere degassing beneath the Western Mediterranean: An integrated model arising from petrological and geophysical data. *Chemical Geology* **262**, 108–120.

Fulignati, P. & Marianelli, P. (2007). Tracing volatile exsolution within the 472 AD 'Pollena' magma chamber of Vesuvius (Italy) from melt inclusion investigation. *Journal of Volcanology and Geothermal Research* **161**, 289–302.

Fulignati, P., Gioncada, A. & Sbrana, A. (1998). The 79 AD Vesuvius magma chamber: a SEM-EDS study of daughter minerals in hypersaline fluid inclusions from cognate syenites. *Neues Jahrbuch für Mineralogie, Monatshefte* **9**, 403–416.

Fulignati, P., Marianelli, M., Proto, M. & Sbrana, A. (2004). Evidences for disruption of a crystallizing front in a magma chamber during caldera collapse: an example from the Breccia Museo unit (Campanian Ignimbrite eruption Italy). *Journal of Volcanology and Geothermal Research* **133**, 141–155.

Gaetani, G. & Grove, T. L. (2003). Experimental constraints on melt generation in the mantle wedge. In: Eiler, J. (ed.) *Inside the Subduction Factory. American Geophysical Union, Geophysical Monograph* **138**, 107–134.

Gaetani, G. A. & Watson, B. E. (2000). Open system behavior of olivine-hosted melt inclusions. *Earth and Planetary Science Letters* **183**, 27–41.

Gaetani, G., O'Leary, J. & Shimizu, N. (2011). Post-entrapment changes to H_2O and CO_2 in olivine-hosted melt inclusions. Goldschmidt 2011 Conference Abstracts. *Mineralogical Magazine* **75**, 879.

Gasperini, D., Blichert-Toft, J., Bosch, D., Del Moro, A., Macera, P. & Albarède, F. (2002). Upwelling of deep mantle material through a plate window: Evidence from the geochemistry of Italian basaltic volcanics. *Journal of Geophysical Research* **107**, 2367, doi:10.1029/2001JB000418.

Ghiara, M. R., Lirer, L. & Munno, R. (1979). Mineralogy and geochemistry of the 'low-potassium series' of the Campania volcanics (South Italy). *Chemical Geology* **26**, 29–49.

Ghiorso, M. S. & Sack, R. O. (1995). Chemical mass transfer in magmatic processes. IV. A revised and internally consistent thermodynamic model for the interpolation and extrapolation of liquid–solid equilibria in magmatic systems at elevated temperatures and pressures. *Contributions to Mineralogy and Petrology* **119**, 197–212.

Giggenbach, W. F. (1996). Chemical composition of volcanic gases. In: Scarpa, R. & Tilling, R. I. (eds) *Monitoring and Mitigation of Volcano Hazards*. Berlin: Springer, pp. 202–226.

Gilg, H. A., Lima, A., Somma, R., Belkin, H. E., De Vivo, B. & Ayuso, R. A. (2001). Isotope geochemistry and fluid inclusion study of skarns from Vesuvius. *Mineralogy and Petrology* **73**, 145–176.

Humphreys, M. C. S., Edmonds, M., Christopher, T. & Hards, V. (2009). Chlorine variations in the magma of Soufrière Hills

Volcano, Montserrat: Insights from Cl in hornblende and melt inclusions. *Geochimica et Cosmochimica Acta* **73(19)**, 5693–5708.

Iacono-Marziano, G., Gaillard, F., Scaillet, B., Pichavant, M. & Chiodini, G. (2009). Role of non-mantle CO_2 in the dynamics of volcano degassing: The Mount Vesuvius example. *Geology* **37**, 319–322, doi:10.1130/G25446A.1.

Ihinger, P. D., Hervig, R. L. & McMillan, P. F. (1994). Analytical methods for volatiles in glasses. In: Carroll, M. R. & Holloway, J. R. (eds) *Volatiles in Magmas. Mineralogical Society of America, Reviews in Mineralogy* **30**, 67–121.

Italiano, F., Martelli, M., Martinelli, G. & Nuccio, M. (2000). Geochemical evidence of melt intrusions along lithospheric faults of the Southern Apennines, Italy: Geodynamic and seismogenic implications. *Journal of Geophysical Research* **105**, 13569–13578.

Jolivet, L., Faccenna, C. & Piromallo, C. (2009). From mantle to crust: Stretching the Mediterranean. *Earth and Planetary Science Letters* **285**, 198–209.

Kelley, K. A. & Cottrell, E. (2009). Water and the oxidation state of subduction zone magmas. *Science* **325**, 605–607.

Lange, R. A. & Carmichael, I. S. E. (1987). Densities of Na_2O–K_2O–CaO–MgO–FeO–Fe_2O_3–Al_2O_3–TiO_2–SiO_2 liquids: New measurements and derived partial molar properties. *Geochimica et Cosmochimica Acta* **51**, 2931–2946.

Le Maitre, R. W., Bateman, P., Dudek, A., Keller, J., Lameyr, J., Le Bas, M. J., Sabine, P. J., Schmid, R., Sørensen, H., Streckeisen, A., Woolley, A. R. & Zanettin, B. (eds) (1989). *A Classification of Igneous Rocks and Glossary of Terms: Recommendations of the International Union of Geological Sciences Subcommission on the Systematics of Igneous Rocks*. Oxford: Blackwell Scientific, 193 p.

Lowenstern, J. B. (1994). Chlorine, fluid immiscibility and degassing in peralkaline magmas from Pantelleria, Italy. *American Mineralogist* **79**, 353–369.

Mangan, M. T. (1990). Crystal size distribution systematics and the determination of magma storage times: the 1959 eruption of Kilauea volcano, Hawaii. *Journal of Volcanology and Geothermal Research* **44**, 295–302.

Mangiacapra, A., Moretti, R., Rutherford, M., Civetta, L., Orsi, G. & Papale, P. (2008). The deep magmatic system of the Campi Flegrei caldera (Italy). *Geophysical Research Letters* **35**, L21304, doi:10.1029/2008GL035550.

Marianelli, P., Métrich, N. & Sbrana, A. (1999). Shallow and deep reservoirs involved in magma supply of the 1944 eruption of Vesuvius. *Bulletin of Volcanology* **61**, 48–63.

Marianelli, P., Sbrana, A., Métrich, N. & Cecchetti, A. (2005). The deep feeding system of Vesuvius involved in recent violent strombolian eruptions. *Geophysical Research Letters* **32**, L02306, doi:10.1029/2004GL021667.

Marianelli, P., Sbrana, A. & Proto, M. (2006). Magma chamber of the Campi Flegrei supervolcano at the time of eruption of the Campanian Ignimbrite. *Geology* **34**, 937–940.

Martelli, M., Nuccio, P. M., Stuart, F. M., Di Liberto, V. & Ellam, R. M. (2008). Constraints on mantle source and interactions from He–Sr isotope variation in Italian Plio-Quaternary volcanism. *Geochemistry, Geophysics, Geosystems* **9**, Q02001, doi:10.1029/2007GC001730.

Massare, D., Métrich, N. & Clocchiatti, R. (2002). High-temperature experiments on silicate melt inclusions in olivine at 1 atm: inference on temperatures of homogenization and H_2O concentrations. *Chemical Geology* **183**, 87–98.

Matzen, A. K., Baker, M. B., Beckett, J. R. & Stolper, E. M. (2011). Fe–Mg partitioning between olivine and high magnesian melts and the nature of Hawaiian parental liquids. *Journal of Petrology* **52**, 1–21.

Maurel, C. & Maurel, P. (1982). Étude expérimentale de la distribution de l'aluminium entre bain silicaté basique et spinelle chromifère. Implications pétrogénétiques: teneur en chrome des spinelles. *Bulletin de Minéralogie* **105**, 197–202.

Métrich, N. & Clocchiatti, R. (1989). Melt inclusion investigation of the volatile behavior in historic alkali basaltic magmas of Etna. *Bulletin of Volcanology* **51**, 185–198.

Moretti, R. (2005). Polymerisation, basicity, oxidation state and their role in ionic modelling of silicate melts. *Annals of Geophysics* **48(4–5)**, 583–608.

Moretti, R. & Ottonello, G. (2003). Polymerization and disproportionation of iron and sulfur in silicate melts: insights from an optical basicity-based approach. *Journal of Non-Crystalline Solids* **323**, 111–119.

Moretti, R. & Papale, P. (2004). On the oxidation state and volatile behaviour in multicomponent gas–melt equilibria. *Chemical Geology* **213**, 265–280.

Mormone, A., Piochi, M., Bellatreccia, F., De Astis, Moretti, R., Della Ventura, G., Cavallo, A. & Mangiacapra, A. (2011). A CO_2-rich magma source beneath the Phlegraen Volcanic District (Southern Italy): Evidence from a melt inclusion study. *Chemical Geology* **287**, 66–80.

Nikogosian, I. K. & van Bergen, M. J. (2010). Heterogeneous mantle sources of potassium-rich magmas in central–southern Italy: Melt inclusion evidence from Roccamonfina and Ernici (Mid Latina Valley). *Journal of Volcanology and Geothermal Research* **197**, 279–302.

Oppenheimer, C., Moretti, R., Kyle, P., Eschenbacher, A., Lowenstern, J. & Hervig, R. (2011). Mantle to surface gas trigger of the alkalic intraplate Erebus volcano, Antarctica. *Earth and Planetary Science Letters* **306**, 261–271.

Orsi, G., Gallo, G. & Zanchi, A. (1991). Simple shearing block resurgence in caldera depressions. A model from Pantelleria and Ischia. *Journal of Volcanology and Geothermal Research* **47**, 1–11.

Orsi, G., Gallo, G., Heiken, G., Wohletz, K., Yu, E. & Bonani, G. (1992). A comprehensive study of the pumice formation and dispersal: the Cretaio tephra of Ischia (Italy). *Journal of Volcanology and Geothermal Research* **53**, 329–354.

Orsi, G., de Vita, S. & Di Vito, M. A. (1996*a*). The restless, resurgent Campi Flegrei nested caldera (Italy): constraints on its evolution and configuration. *Journal of Volcanology and Geothermal Research* **74**, 179–214.

Orsi, G., Piochi, M., Campajola, L., D'Onofrio, A., Gialanella, L. & Terrasi, F. (1996*b*). ^{14}C geochronological constraints for the volcanic history of the island of Ischia (Italy) over the last 5,000 years. *Journal of Volcanology and Geothermal Research* **71**, 249–257.

Orsi, G., Petrazzuoli, S. & Wohletz, K. (1999*a*). Mechanical and thermo-fluid behaviour during unrest episode at the Campi Flegrei caldera (Italy). *Journal of Volcanology and Geothermal Research* **91**, 453–470.

Orsi, G., Patella, D., Piochi, M. & Tramacere, A. (1999*b*). Magnetic modeling of the Phlegraean Volcanic District with extension to the Ponza archipelago, Italy. *Journal of Volcanology and Geothermal Research* **91**, 345–360.

Orsi, G., de Vita, S., Di Vito, M., Isaia, R., Nave, R. & Heiken, G. (2003). Facing volcanic and related hazards in the Neapolitan area. In: Heiken, G., Fakundiny, R. & Sutter, J. (eds) *Earth Sciences in the Cities: A Reader. American Geophysical Union, Special Publication Series* **56**, 121–170.

Ottonello, G., Moretti, R., Marini, L. & Vetuschi Zuccolini, M. (2001). Oxidation state of iron in silicate glasses and melts: a thermochemical model. *Chemical Geology* **174**, 157–179.

Pabst, S., Wörner, G., Civetta, L. & Tesoro, R. (2008). Magma chamber evolution prior to the Campania Ignimbrite and Neapolitan Yellow Tuff eruptions (Campi Flegrei, Italy). *Bulletin of Volcanology* **70**, 961–976.

Paoletti, V., Di Maio, R., Cella, F., Florio, G., Motschka, K., Roberti, N., Secomandi, M., Supper, R., Fedi, M. & Rapolla, A.

(2009). The Ischia volcanic island (Southern Italy): Inferences from potential field data interpretation. *Journal of Volcanology and Geothermal Research* **179**, 69–86.

Papale, P., Moretti, R. & Barbato, D. (2006). The compositional dependence of the saturation surface of $H_2O + CO_2$ fluids in silicate melts. *Chemical Geology* **229(1–3)**, 78–95.

Pappalardo, L., Piochi, M., D'Antonio, M., Civetta, L. & Petrini, R. (2002). Evidence for multi-stage magmatic evolution during the past 60 kyr at Campi Flegrei (Italy) deduced from Sr, Nd and Pb isotope data. *Journal of Petrology* **43**, 1415–1434.

Peccerillo, A. (2005). *Plio-Quaternary Volcanism in Italy—Petrology, Geochemistry, Geodynamics*. Heidelberg: Springer, 365 p.

Petrelli, M., Poli, G., Perugini, D. & Peccerillo, A. (2005). Petrograph: a new software to visualize, model, and present geochemical data in igneous petrology. *Geochemistry, Geophysics, Geosystems* **6**, Q07011, doi:10.1029/2005GC000932.

Piochi, M., Civetta, L. & Orsi, G. (1999). Mingling in the magmatic system of Ischia (Italy) in the past 5 ka. *Mineralogy and Petrology* **66**, 227–258.

Piochi, M., Bruno, P. P. & De Astis, G. (2005). Relative roles of rifting tectonics and magma ascent processes: Inferences from geophysical, structural, volcanological, and geochemical data for the Neapolitan volcanic region (southern Italy). *Geochemistry, Geophysics, Geosystems* **6**, Q07005, doi:10.1029/2004GC000885.

Plank, T., Cooper, L. B. & Manning, C. E. (2009). Emerging geothermometers for estimating slab surface temperatures. *Nature Geoscience* **2**, 611–615.

Quareni, F., Moretti, R., Piochi, M. & Chiodini, G. (2007). Modeling of the thermal state of Mt. Vesuvius from 1631 AD to present and the role of CO_2 degassing on the volcanic conduit closure after the 1944 AD eruption. *Journal of Geophysical Research—Solid Earth* **112**, B03202.

Roedder, E. (1984). *Fluid Inclusions. Mineralogical Society of America, Reviews in Mineralogy* **12**, , 644 p.

Roeder, P. L. & Emslie, R. F. (1970). Olivine–liquid equilibrium. *Contributions to Mineralogy and Petrology* **29**, 275–289.

Roselieb, K. & Jambon, A. (2002). Tracer diffusion of Mg, Ca, Sr, and Ba in Na-aluminosilicate melts. *Geochimica et Cosmochimica Acta* **66**, 109–123.

Rust, A. C., Cashman, K. V. & Wallace, P. J. (2004). Magma degassing buffered by vapor flow through brecciated conduit margins. *Geology* **32**, 349–352.

Santacroce, R., Cioni, R., Marianelli, P., Sbrana, A., Sulpizio, R., Zanchetta, G., Donahue, D. J. & Joron, J. L. (2008). Age and whole rock–glass compositions of proximal pyroclastics from the major explosive eruptions of Somma–Vesuvius: A review as a tool for distal tephrostratigraphy. *Journal of Volcanology and Geothermal Research* **177**, 1–18.

Sbrana, A., Fulignati, P., Marianelli, P., Boyce, A. J. & Cecchetti, A. (2009). Exhumation of an active magmatic–hydrothermal system in a resurgent caldera environment: the example of Ischia (Italy). *Journal of the Geological Society, London* **166**, 1061–1073.

Scaillet, B. & Pichavant, M. (2005). A model of sulphur solubility for hydrous mafic melts: Application to the determination of magmatic fluid compositions of Italian volcanoes. *Annals of Geophysics* **48**, 671–698.

Sepe, V., Atzori, S. & Ventura, G. (2007). Subsidence due to crack closure and depressurization of hydrothermal systems: a case study from Mt. Epomeo (Ischia Island, Italy). *Terra Nova* **19**, 127–132.

Severs, M. J. (2007). Applications of melt inclusions to problems in igneous petrogenesis, MSc dissertation, Virginia Tech, Blacksburg, VA, 118 pp.

Signorelli, S., Vaggelli, G., Francalanci, L. & Rosi, M. (1999*a*). Origin of magmas feeding the Plinian phase of the Campanian Ignimbrite eruption (Phlegrean Fields Italy): constraints based on matrix glass and glass inclusion compositions. *Journal of Volcanology and Geothermal Research* **91**, 199–220.

Signorelli, S., Vaggelli, G. & Romano, C. (1999*b*). Pre-eruptive volatile (H_2O, F, Cl and S) contents of phonolitic magmas feeding the 3550-year-old Avellino eruption from Vesuvius, southern Italy. *Journal of Volcanology and Geothermal Research* **93**, 237–256.

Simakin, A. G., Salova, T. P. & Bondarenko, G. V. (2012). Experimental observation of magmatic melt oxidation by CO_2 fluxing. *Petrology* **20**, 593–606.

Spilliaert, N., Allard, P., Métrich, N. & Sobolev, A. V. (2006). Melt inclusion record of the conditions of ascent, degassing, and extrusion of volatile-rich alkali basalt during the powerful 2002 flank eruption of Mount Etna (Italy). *Journal of Geophysical Research* **111**, B04203, doi:10.1029/2005JB003934.

Symonds, R. B. & Reed, M. H. (1993). Calculation of multicomponent chemical equilibria in gas–solid–liquid systems: calculation methods, thermochemical data, and applications to studies of high-temperature volcanic gases with examples from Mount St. Helens. *American Journal of Science* **293**, 758–864.

Tonarini, S., Leeman, W. P., Civetta, L., D'Antonio, M., Ferrara, G. & Necco, A. (2004). B/Nb and $\delta^{11}B$ systematics in the Phlegrean Volcanic District, Italy. *Journal of Volcanology and Geothermal Research* **133**, 123–139, doi:10.1016/S0377-0273(03)00394-9.

Tonarini, S., D'Antonio, M., Di Vito, M. A., Orsi, G. & Carandente, A. (2009). Geochemical and B–Sr–Nd isotopic evidence for mingling and mixing processes in the magmatic system that fed the Astroni volcano (4·1–3·8 ka) within the Campi Flegrei caldera (southern Italy). *Lithos* **107**, 135–151, doi:10.1016/j.lithos.2008.09.012.

Vetere, F., Botcharnikov, R. E., Holtz, F., Behrens, H. & De Rosa, R. (2011). Solubility of H_2O and CO_2 in shoshonitic melts at 1250°C and pressures from 50 to 400 MPa: Implications for Campi Flegrei magmatic systems. *Journal of Volcanology and Geothermal Research* **202**, 251–261, doi:10.1016/j.jvolgeores.2011.03.002.

Vezzoli, L. (ed.) (1988). *Island of Ischia. CNR Quaderni de 'La ricerca scientifica'* **114-10**, , 122 p.

Vigouroux, N., Wallace, P. J. & Kent, A. J. R. (2008). Volatiles in high-K magmas from the Western Trans-Mexican Volcanic Belt: Evidence from fluid fluxing and extreme enrichment of the mantle wedge by subduction processes. *Journal of Petrology* **49(9)**, 1589–1618, doi:10.1093/petrology/egn039.

Villemant, B. (1988). Trace element evolution in the Phlegrean Fields (Central Italy): fractional crystallization and selective enrichment. *Contributions to Mineralogy and Petrology* **98**, 169–183.

Webster, J. D., Raia, F., Tappen, C. & De Vivo, B. (2003). Pre-eruptive geochemistry of the ignimbrite-forming magmas of the Campanian Volcanic Zone, Southern Italy, determined from silicate melt inclusions. *Mineralogy and Petrology* **79**, 99–125.

Zhang, Y. (2008). *Geochemical Kinetics*. Princeton, NJ: Princeton University Press, 631 p.

Zollo, A., Maercklin, N., Vassallo, M., Dello Iacono, D., Virieux, J. & Gasparini, P. (2008). Seismic reflections reveal a massive melt layer under Campi Flegrei volcanic field. *Geophysical Research Letters* **35**, L12306, doi:10.1029/2008GL034242.